Agricultural Water Management 288 (2023) 108489

Contents lists available at ScienceDirect

Agricultural Water Management

journal homepage: www.elsevier.com/locate/agwat

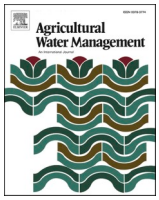

Performance evaluation of a low-cost thermal camera for citrus water status estimation

S. Pappalardo [a], S. Consoli [a], G. Longo-Minnolo [a,*], D. Vanella [a], D. Longo [a], S. Guarrera [a], A. D'Emilio [a], J.M. Ramírez-Cuesta [a,b]

[a] Dipartimento di Agricoltura, Alimentazione e Ambiente (Di3A), Università degli Studi di Catania, Via S. Sofia, 100, Catania 95123, Italy
[b] Department of Ecology, Desertification Research Centre (CIDE-CSIC-UV-GV), Moncada, 46113 Valencia, Spain

ARTICLE INFO

Handling Editor - Dr. B.E. Clothier

Keywords:
Infrared thermography
Crop water stress index
Deficit irrigation
Smartphone application
Precision irrigation

ABSTRACT

The main limitation of conventional methods generally used for monitoring the crop water stress lies in the expenditure of time and laboriousness (e.g., stem water potential, Ψ_{stem}). In this sense, infrared thermography can assist to identify the crop water status for precise irrigation purposes. However, this method requires high cost equipment and heavy systems for real-time analysis of the results. The aim of this research was to evaluate the reliability of a portable low-cost sensor (FLIR One Pro), connectable to a smartphone, for determining the water status of orange trees subjected to different treatments (i.e., full irrigation versus regulated deficit irrigation with or without soil mulching). The thermal information obtained from FLIR One Pro was compared with the data acquired with a professional thermal camera (Optris Xi 400) for two consecutive years (2021–2022). In addition, the reliability of the low-cost sensor was assessed, in respect to the loss of accuracy due to the sensor's price reduction, in identifying the crop water stress index (CWSI) and the upper and lower baselines. A good agreement was obtained between the canopy temperature (T_c) and the references leaves temperatures (dry leaf, T_d; and wet leaf, T_w) provided by both sensors, resulting in coefficient of determination (R^2) of 0.89, 0.82 and 0.75, respectively. The CWSI comparing the two sensors provided a R^2 of 0.75. No influence of the agro-meteorological conditions and overheating of the low-cost sensor on the T_c was found, however it is advisable to keep the low-cost sensor under homogeneous weather conditions during the acquisition process. No correlation was found between the CWSI and the Ψ_{stem}, due to the isohydric behavior of citrus species. Finally, this study opens new insights for spreading the use of low-cost thermal sensors for speeding up the crop water status monitoring under field conditions and supporting the adoption of precision irrigation criteria.

1. Introduction

Nowadays, despite irrigation represents the biggest user of freshwater on Earth, still a large proportion of water is wasted due to the improper irrigation management (Cohen et al., 2017). Furthermore, water supply for irrigation is expected to decrease in the next future due to the occurrence of frequent droughts and the increased competition from the industrial sector (Alvino and Marino, 2017). Hence, there is a need of developing and implementing sustainable approaches for optimizing the water use efficiency by the irrigated agriculture sector (Rud et al., 2014; Cohen et al., 2017; Han et al., 2018).

In this sense, the determination of crop water status plays a key role for supporting the adoption of sustainable irrigation practices and the implementation of precision agriculture criteria (Cohen et al., 2017; Han et al., 2018). Traditionally, crop water status is derived using both soil and/or plant-based measurement approaches. Specifically, conventional methods used for monitoring the soil-water relationships consist in determining the soil moisture and/or matric potential at the root-zone level by local measurements, e.g., based on time or frequency domain reflectometry. On the other hand, plant-based approaches include measurements of stomatal conductance, leaf or stem water potential (Ψ_{stem}), and relative water content (Jones, 2004). However, all these methods suffer to be not always representative of the soil heterogeneity of the field (Clarke, 1997; Motisi et al., 2012). Moreover, they are time consuming, labor intensive and some of them are destructive, being used more for research purposes rather than for irrigation planning (Ihuoma and Madramootoo, 2017; Saitta et al., 2021).

In order to overcome some of these limitations, remote/proximal

* Corresponding author.
E-mail address: giuseppe.longominnolo@phd.unict.it (G. Longo-Minnolo).

https://doi.org/10.1016/j.agwat.2023.108489
Received 22 May 2023; Received in revised form 20 August 2023; Accepted 22 August 2023
Available online 26 August 2023

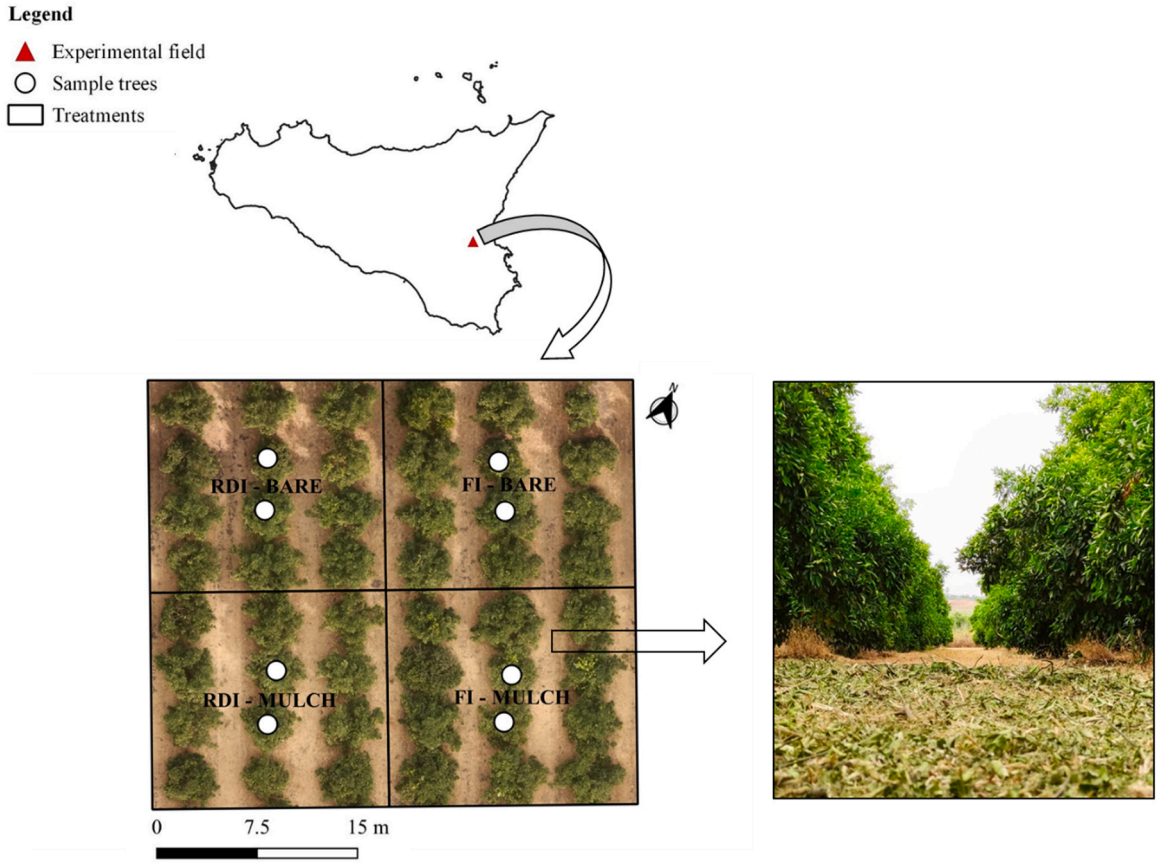

Fig. 1. Location of the study area and indication of the experimental treatments under study. FI and RDI refer to full irrigation and regulated deficit irrigation, respectively; whereas Mulch and Bare identify organic mulching substrate and bare soil conditions, respectively.

sensing techniques may offer alternative methods for detecting the crop water status in a spatially distributed and time-responsive manner (e.g., Consoli and Vanella, 2014; Ihuoma and Madramootoo, 2017; Mwinuka et al., 2021). In particular, plant responses to biotic and abiotic stresses cause biophysical and biochemical changes, such as reducing biomass and chlorophyll content, changes in internal leaf structures and canopy temperature (T_c) (Mahajan et al., 2014). These responses are easily and non-destructive detectable throughout the use of sensors, based both on multispectral and/or infrared thermal data (Abdulridha et al., 2018; Ampatzidis et al., 2019; Hillnhütter et al., 2011; Morlin Carneiro et al., 2020). In addition, multispectral and thermal sensors have gained popularity in the last years due to the improvements in sensor technology and reduction of their costs (Khanal et al., 2017; Shafian et al., 2018).

Several authors have recognized infrared thermography as a useful tool for irrigation scheduling (Berni et al., 2009; Cohen et al., 2005, 2017; Jones et al., 2004; Meron et al., 2010). In fact, temperature is a fundamental environmental variable that plays an essential role in the plant physiological processes. Specifically, T_c is a good indicator of water status due to its inverse relationship with canopy water loss rate which is closely related to stomatal conductance. Thus, temperature-based indices could be a quick and practical way to assess and estimate crop water status by depicting the plant water content (Ballester et al., 2013; Mangus et al., 2016; Möller et al., 2007). Nevertheless, there are multiple factors that increase the uncertainty of T_c measurements. In this sense, sudden agrometeorological variations, such as in air temperature (T_a), solar radiation (R_s), vapor pressure deficit (VPD) and especially in wind speed (WS) have a direct effect on the thermal response of the canopy (García-Tejero et al., 2012, 2017; Jones, 2004; Petrie et al., 2019; Ramírez-Cuesta et al., 2022b). Furthermore, it also depends on the specific physiological responses of the plant combined with the soil water deficit conditions (e.g. isohydric or anishydric behavior), and on the leaf anatomy (large versus lanceolate leaves) (Ramírez-Cuesta et al., 2022a). Therefore, to mitigate the impact of these components on the actual crop water stress condition, stress indices have been developed. Among these indices, the crop water stress index (CWSI; Jackson et al., 1981) is the most widely used and it is based on the relationship between T_c to T_a difference, and the VPD. Specifically, the CWSI approach uses the surface energy balance theory, which separates the net radiation on the canopy from sensible heat (thermal content of the air) and latent heat fluxes consumed for transpiration. This index has been successfully exploited for monitoring the crop water status, including in vineyard (Costa et al., 2013; García-Tejero et al., 2016; Grant et al., 2016; King et al., 2020; Pou et al., 2014; Gutiérrez et al., 2021), citrus (Gonzalez-Dugo et al., 2014), cherry (Blaya-Ros et al., 2020) almond (García-Tejero et al., 2012, 2016), peach (Ramírez-Cuesta et al., 2022a; Bellvert et al., 2014) and olive groves (García-Tejero et al., 2017).

As regards, the thermal images acquisition, in the last decades, several low-cost sensors have been developed (Ramírez-Cuesta et al., 2022a). These sensors could be an alternative tool to obtain satisfactory results instead of using high resolution cameras, due to their lower price, simpler user interface and, therefore, better feedback to be inserted in the business context (Puértolas et al., 2018; García-Tejero et al., 2018). However, these advantages are accompanied by a reduction of the quality of the data these sensors provide (e.g. accuracy, operating temperature and thermal sensitivity) or the materials they are made of (Giordano et al., 2021). These sensors have been applied to evaluate the water status of several crops, such as maize (Fisher and Kebede, 2010), sugar beet (Bendig et al., 2012), black bean (Khorsand et al., 2021), tomato (Takács et al., 2018), vineyard (Petrie et al., 2019), cherry (Blaya-Ros et al., 2020), and eggplant (Mwinuka et al., 2021). However,

Table 1
Treatments established in the present study as combination between the two factors considered at the study area. FI and RDI refer to full irrigation and regulated deficit irrigation, respectively; whereas Mulch and Bare identify organic mulching substrate and bare soil conditions, respectively.

Treatment	Irrigation management	Soil management
FI-Bare	Full irrigation	Bare soil
FI-Mulch	Full irrigation	Mulching
RDI-Bare	Regulated deficit irrigation	Bare soil
RDI-Mulch	Regulated deficit irrigation	Mulching

only few authors have addressed the comparison between the T_c provided by low-cost sensors with those derived from professional cameras (García-Tejero et al., 2018; Noguera et al., 2020; Giménez-Gallego et al., 2021; Irsyad et al., 2022), as well as the implications that T_c differences among sensors have on the calculation of the CWSI (Carrasco-Benavides et al., 2020). Moreover, particular attention needs to be paid when acquiring the T_c for implementing the CWSI. In fact, overestimates of CWSI can be obtained when the upper and lower baselines are not accurately defined. Specifically, uncertainties in CWSI may be caused by higher T_c values acquired on the field (e.g., considering only the sunny side of the tree) or lower values when T_c is measured in air resulting in more stressful conditions than under the real conditions (Ramírez-Cuesta et al., 2022a). Additionally, thermal images may be affected by multiple factors, including the characteristics of the thermal camera characteristics, the meteorological conditions, and several sources of uncertainty related to the emitted and reflected thermal radiation (Khanal et al., 2017). In this framework, the main aim of this study was to evaluate the feasibility of using low-cost thermal sensors and understanding if the loss of accuracy due to the sensor's price reduction is bearable to perform studies of crop water status. Specific objectives of this study were: (i) to assess the performance of the thermal camera FLIR One Pro for smartphone compared to the professional thermal camera Optris Xi 400 for detecting T_c, as well as for identifying the upper and lower baselines and determining the CWSI; (ii) to evaluate the influence of the agrometeorological conditions on the sensors sensitivity for acquiring the thermal images; and (iii) to assess the water status of citrus crops by using thermal data with respect to the traditional physiological parameters (i.e., Ψ_{stem}).

2. Material and methods

2.1. Study area

The experimental site is an orange orchard located in Southern Italy (Eastern Sicily, Lentini; 37°20'12.65" N, 14°53'33.04" E, WGS84; Fig. 1), managed by "Centro di Ricerca Olivicoltura, Frutticoltura e Agrumicoltura" of the Italian Council for Agricultural Research and Agricultural Economics Analyses (CREA-OFA). Orange trees (*Citrus sinensis* (L.) Osbeck cv "Tarocco Sciara") were planted in 2010, with trees and rows spacing of 4 and 6 m, respectively. In 2022, average (± standard error, SE) tree height, trunk and canopy diameters were of 3.0 m (± 0.3 m), 0.15 m (± 0.02 m) and 3.2 m (± 0.3 m), respectively. The climate of the area is hot-summer Mediterranean, with warm and dry summers. Specifically, during the period 2002–2022, average T_a (°C), cumulated annual precipitation (mm) and reference evapotranspiration (ET_0; mm) values were of 18.3 °C, 577 mm and 1264 mm, respectively (data provided by a weather station located about 2 km far from the study site, managed by Servizio Informativo Agrometeorologico Siciliano, SIAS; http://www.sias.regione.sicilia.it/). The soil at the study area has a sandy loam texture, with field capacity and wilting point values of 0.28 and 0.14 cm^3 cm^{-3}, respectively (Consoli et al., 2017).

At the experimental orchard, a two-factorial trial was designed. The two analyzed factors were (i) irrigation, and (ii) soil management. Irrigation management included a full irrigation (FI) treatment, where irrigation rate corresponded to 100% of crop evapotranspiration (ET_c) and a regulated deficit irrigation (RDI) treatment, supplied with the 100% of ET_c, except during the II phenological stage (fruit growth, starting from Day Of the Year, DOY_s 202–258 in 2021 and 214–259 in 2022), when irrigation rate was reduced to 50% of ET_c (Saitta et al., 2020; Vanella et al., 2021). The daily ET_c estimates were derived using the single crop coefficient (K_c) FAO-56 approach (Allen et al., 1998), by multiplying the daily ET_0 (i.e., calculated using the agrometeorological data provided by the nearest SIAS weather station) and the seasonal K_c for orange orchard adjusted for the local conditions (i.e., 0.7 as observed by Consoli and Papa, 2013). Treatments were micro-irrigated with a surface drip irrigation system, which included 12 emitters per trees; each dripper emitted a flow rate of 4 L h^{-1}. According to the irrigation management under study (FI versus RDI), irrigation volumes were applied 3 times for week during the irrigation seasons 2021 (from DOY 186 to DOY 258) and 2022 (from DOY 164 to DOY 259). In particular, cumulative irrigation volumes of 183 and 256 mm were registered under the FI in 2021 and 2022, respectively, reaching average water savings of 23% under RDI conditions.

Table 3
Specifications of the two thermal sensors used in the present study (i.e., FLIR One Pro and Optris Xi 400).

Parameter	FLIR One Pro	Optris Xi 400
Optical resolution	640 × 480	382 × 288
Object temperature range	-20–400 °C	-20–900 °C
Spectral range	8–14 μm	8–14 μm
Accuracy	±3 °C	±2 °C
Operating temperature	0–35 °C	0–50 °C
Thermal sensitivity	150 mK	80 mK
Field Of View (FOV)	55° x 43°	53° x 38°
Emissivity setting	0.60–0.95	0.1–1.1
Acquisition software	FLIR One (App for smartphone)	PIX Connect (PC Windows)
Price (currently)	~ 450 $	~ 3000 $

Table 2
Minimum and maximum values of the agrometeorological variables registered during each thermal acquisition campaign (R_s = solar radiation; T_a = air temperature; RH = relative humidity; WS = wind speed; VPD = vapor pressure deficit; and ET_0 = reference evapotranspiration).

Date	DOY	Temporal interval	R_s (W m^{-2})	T_a (ºC)	RH (%)	WS (m s^{-1})		VPD (kPa)	ET_0 (mm)
Jul 22, 2021	203	11:50–12:31	693–973	33.4–34.6	38–42	2.0–2.5	3.0–3.4		0.6–0.8
Jul 29, 2021	210	11:52–12:42	775–938	39.9–42.6	16–24	1.3–2.3	5.6–7.0		0.7–0.9
Aug 24, 2021	236	11:48–12:35	772–852	34.8–36.4	14–18	1.8–4.8	4.0–4.4		0.8–0.9
Sep 1, 2021	244	12:05–12:53	552–744	30.6–31.5	47–55	3.4–4.3	2.0–2.4		0.5–0.7
Sep 21, 2021	264	11:55–12:45	622–794	31.1–31.8	53–59	1.4–2.0	1.8–2.2		0.5–0.6
Jun 28, 2022	179	11:58–12:46	793–941	39.6–41.0	20–22	1.4–1.9	5.6–6.2		0.7–0.9
Jul 12, 2022	193	12:00–12:43	824–970	34.5–35.0	23–26	1.7–2.2	4.1–4.3		0.7–0.8
Jul 19, 2022	200	12:02–12:50	800–928	34.2–34.7	38–40	1.8–2.1	3.2–3.4		0.7–0.8
Aug 2, 2022	214	12:00–12:40	789–939	35.5–37.0	17–23	1.3–2.4	4.4–5.2		0.7–0.8
Sep 20, 2022	263	12:05–12:50	538–784	32.1–35.7	46–49	1.0–2.3	1.8–4.3		0.5–0.7

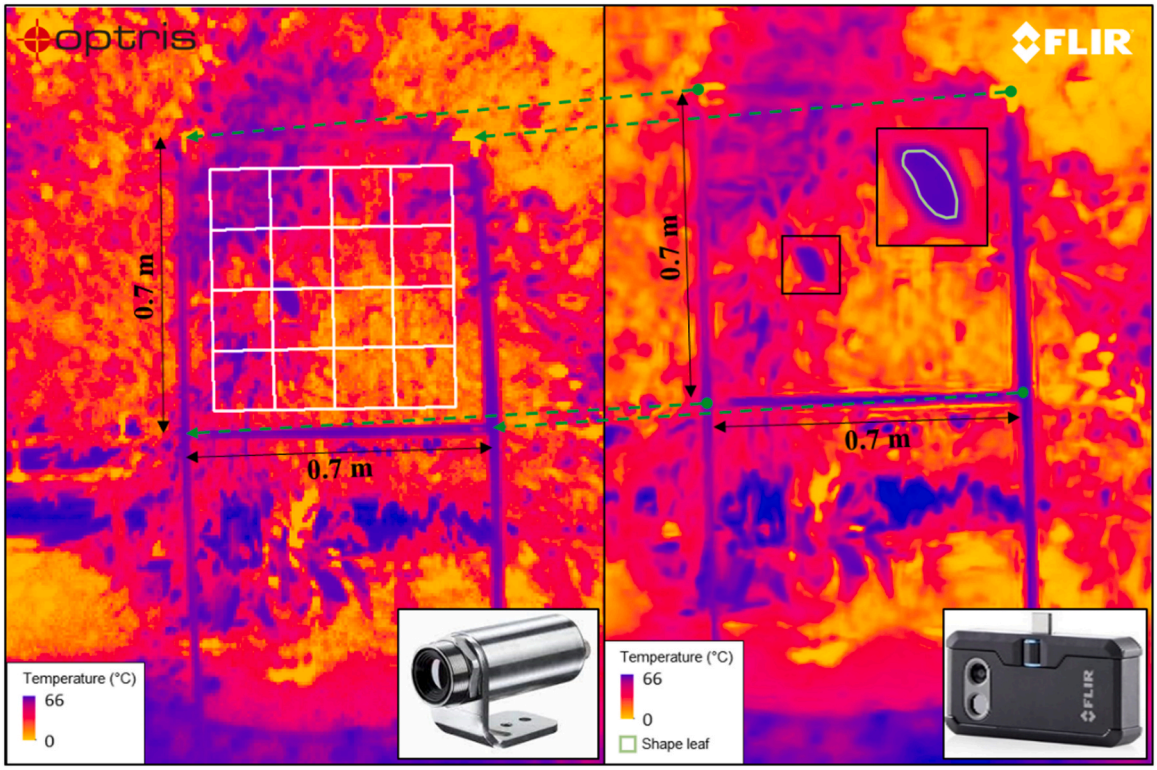

Fig. 2. Spatial resolution differences between FLIR and Optris and fishnet mask used for statistical sensors comparisons together with an example of creation of the leaf shape. The pictures refer to the thermal acquisitions collected on Jul 29, 2021 at FI-Mulch treatment.

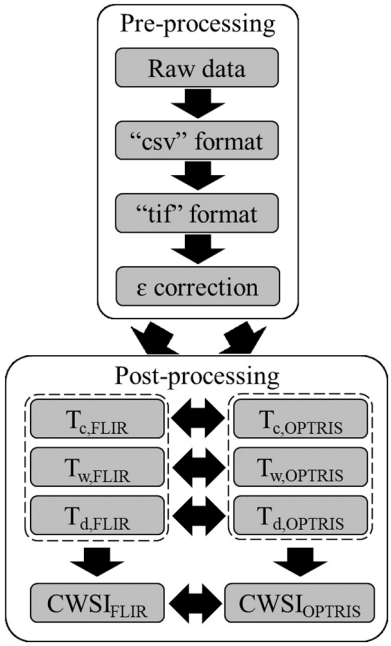

Fig. 3. Pre-processing and post-processing workflow after the field acquisition.

Soil management included a bare soil strategy and the application of organic mulching with residues of pruning waste and weeds. The thickness of the organic mulching substrate was 0.02 and 0.07 m, with a wet weight per plot of 720 and 1625 kg for 2021 and 2022 seasons, respectively. The size of each plot is of about 18 × 15 m, with nine trees inside.

From the combination of the irrigation and soil management strategies, 4 treatments were established as reported in Table 1 and Fig. 1. Two sample trees per treatment (n = 8) were selected in order to assess the main evaluations and analyses during the study.

2.2. Thermal data acquisition and processing

A thermal acquisition campaign was performed during the years 2021 and 2022, with a total of 10 sample dates. Table 2 shows, for each measurement date, the minimum and maximum values of the agro-meteorological variables registered during the temporal interval of each single thermal campaign acquisition, i.e., R_s (Wm^{-2}) T_a (°C), relative humidity (RH; %), WS ($m\ s^{-1}$), VPD (kPa) and ET_0 (mm). These values were acquired by an automatic weather station located at the study site. Details on the sensors are described in Vanella et al. (2022).

Two different proximal thermal sensors were used for the thermal measurements, i.e. the low-cost camera FLIR One Pro (Teledyne FLIR LLC, Arlington, Virginia) and the professional camera Optris Xi 400 (Optris GmbH, Berlin, Germany). The main specifications of the two sensors are given in Table 3. Note that the calibration file associated with the serial number of each commercial thermal camera (i.e., individually calibrated in laboratory) supplied by the manufacturer guarantees that the performances indicated in the sensor's manuals are respected.

During each acquisition period, four thermal images (T_c; T_d, dry leaf temperature; T_w, wet leaf temperature; and $T_{body\ FLIR}$, body FLIR temperature) per sample tree per sensor were acquired in the Eastern (sunny) part of the canopy. The thermal image acquisition was performed with the sensors located 4 m far from the plant canopy at a height of 1.5 m, using a tripod support, and setting emissivity values of 0.95 and 0.98 for FLIR One Pro and Optris Xi 400 sensors, respectively. These thermal photographs were used for performing a comparison between the T_c acquired by each sensor. To facilitate the comparison between the thermal images obtained with the two sensors, a wooden frame of 0.7 × 0.7 m was used as a reference (placed in the canopy with

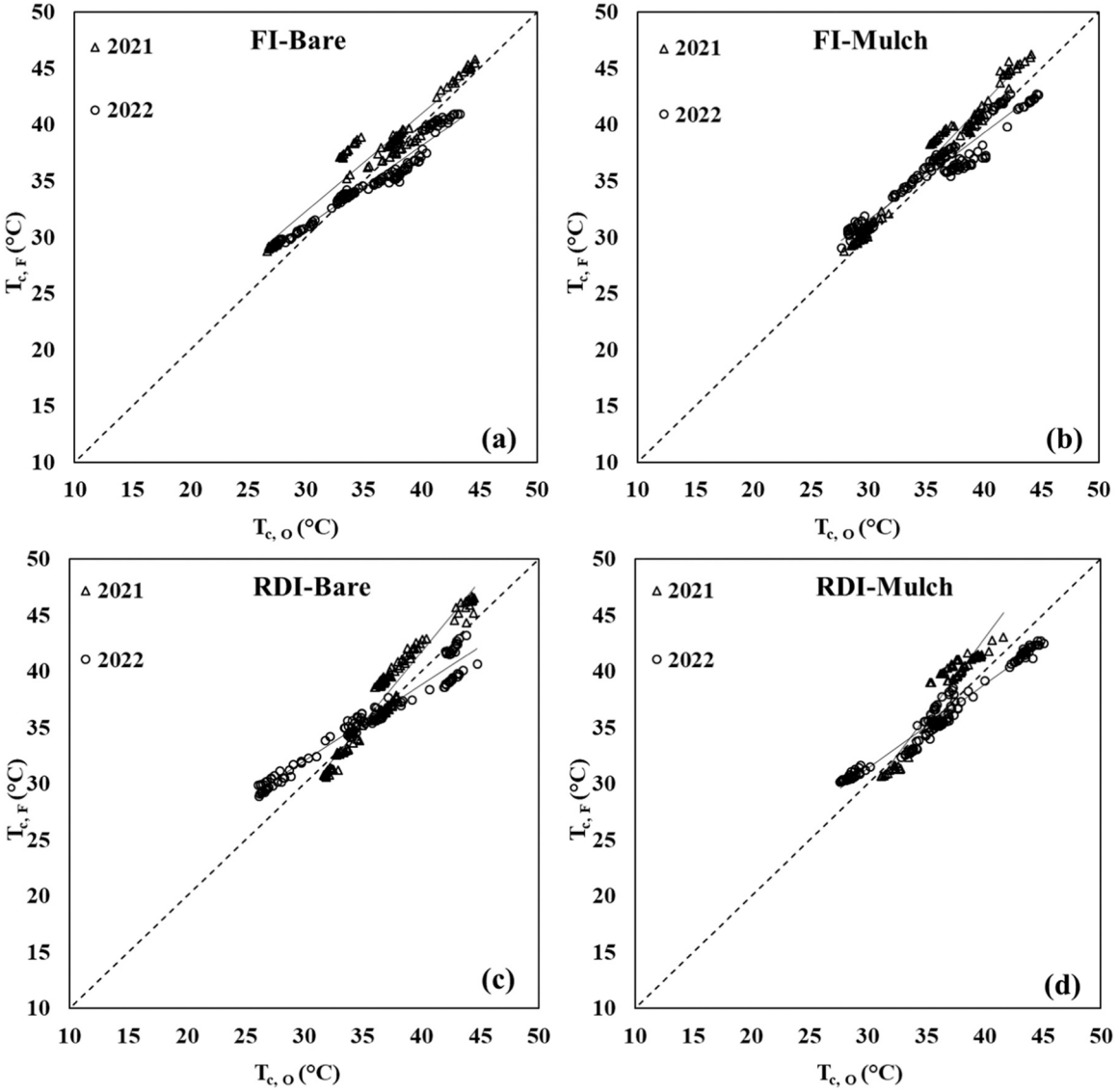

Fig. 4. Relationships between canopy temperature acquired with Optris Xi 400 ($T_{c,O}$) and FLIR One Pro sensors ($T_{c,F}$), respectively, for the different treatments applied at the study area and during the years 2021–2022: (a) FI-Bare, (b) FI-Mulch, (c) RDI-Bare, (d) RDI-Mulch. FI and RDI refer to full irrigation and regulated deficit irrigation; whereas Mulch and Bare identify organic mulching substrate and bare soil conditions, respectively.

its center at a height of 1.5 m, Fig. 2). The utilization of this frame allowed increasing the number of sensors comparison points (16 regions within each sample tree), overcoming the limitations in the number of sampling trees due to the FLIR One Pro sensor battery duration.

The calculation of CWSI requires the use of two limits to standardize for the effects of the atmospheric conditions on canopy transpiration and temperature (Idso et al., 1981; Jackson et al., 1981). These thresholds include non-water stress (LL) baselines and non-transpiration (UL) baselines. The procedure for LL and UL baselines determination implies: (i) the acquisition of the non-transpiring dry leaf temperature (T_d), in which the stomata were completely closed by covering the leaf with petroleum jelly (vaseline) on both sides; and (ii) the acquisition of the wet leaf temperature (T_w), corresponding to a condition of completely open stomata, obtained by spraying the leaf with water and soap on both sides (Ramírez-Cuesta el, 2022a). For this purpose, two closer thermal images per tree (0.15 m far from the tree canopy) were acquired in order to determine the CWSI thresholds (i.e. LL and UL). Thus, CWSI was calculated as:

$$CWSI = \frac{T_c - T_w}{T_d - T_w} \quad (1)$$

where T_w and T_d are the lowest wet leaf temperature and the highest dry leaf temperature for each date, respectively. When the plant canopy is fully transpiring, the leaf temperature is a few degrees below the temperature of the overlying air layer and the CWSI is close to 0 (stomata are opened). Conversely, as transpiration decreases, leaf temperature increases and can reach a few degrees above the temperature of the overlying air, with CWSI equal to 1 when transpiration is totally halted. The CWSI was, thus, calculated using the lowest T_w and the highest T_d for each date.

Moreover, during the thermal acquisition campaign in 2022, the temperature of the FLIR sensor body was monitored by the Optris camera in order to identify a possible overheating of the low-cost sensor. The sensor was always kept under shade conditions except during the image acquisition. This choice was made because the Optris sensor has a clear polished steel sensor body, less sensitive to overheating. The overall thermal acquisition duration for each sample date was around 45 min, from about 12:00–12:45 (CET) (Table 2). During the acquisition process, no rain or irrigation occurred and cloudy days have been avoided.

The raw thermal data processing procedure includes the following

Table 4
Statistical indicators of the relationships obtained for canopy (T_c) and wet (T_w) and dry (T_d) leaves temperatures between FLIR and Optris sensors at the treatments under study. Asterisks indicate statistically significant relationships ($p < 0.05$).

Year	Treatment	Parameter	Slope (a)	Intercept (b, °C)	R^2	RMSE (°C)	PBIAS (%)
2021	FI-Bare	T_c*	0.87	6.22	0.93	2.03	-4.12
		T_w*	0.68	11.92	0.93	2.24	-4.12
		T_d*	0.89	5.07	0.97	1.16	-1.07
	FI-Mulch	T_c*	1.09	1.91	0.98	1.77	-4.20
		T_w*	0.91	5.38	0.90	2.98	-8.36
		T_d*	1.07	1.76	0.98	1.45	-2.58
	RDI-Bare	T_c*	1.27	9.07	0.93	1.77	-2.52
		T_w*	0.92	3.49	0.85	1.42	-4.11
		T_d*	1.04	0.87	0.84	1.33	-1.50
	RDI-Mulch	T_c*	1.38	12.50	0.93	2.24	-4.39
		T_w*	1.53	14.94	0.84	2.43	-4.38
		T_d*	1.14	4.79	0.91	1.97	-2.35
2022	FI-Bare	T_c*	0.72	9.31	0.95	1.66	1.85
		T_w*	0.75	7.93	0.81	1.63	-4.95
		T_d*	0.52	18.98	0.80	2.68	2.41
	FI-Mulch	T_c*	0.78	8.18	0.93	1.47	-0.35
		T_w*	0.77	8.06	0.80	2.56	-6.93
		T_d*	0.82	6.65	0.86	2.16	2.70
	RDI-Bare	T_c*	0.68	11.59	0.96	2.10	-0.95
		T_w*	1.00	2.92	0.91	3.28	-12.05
		T_d*	0.70	11.86	0.94	2.17	2.66
	RDI-Mulch	T_c*	0.74	9.10	0.97	1.49	0.39
		T_w*	0.96	3.83	0.86	2.93	-9.59
		T_d*	0.54	17.96	0.91	3.09	4.07

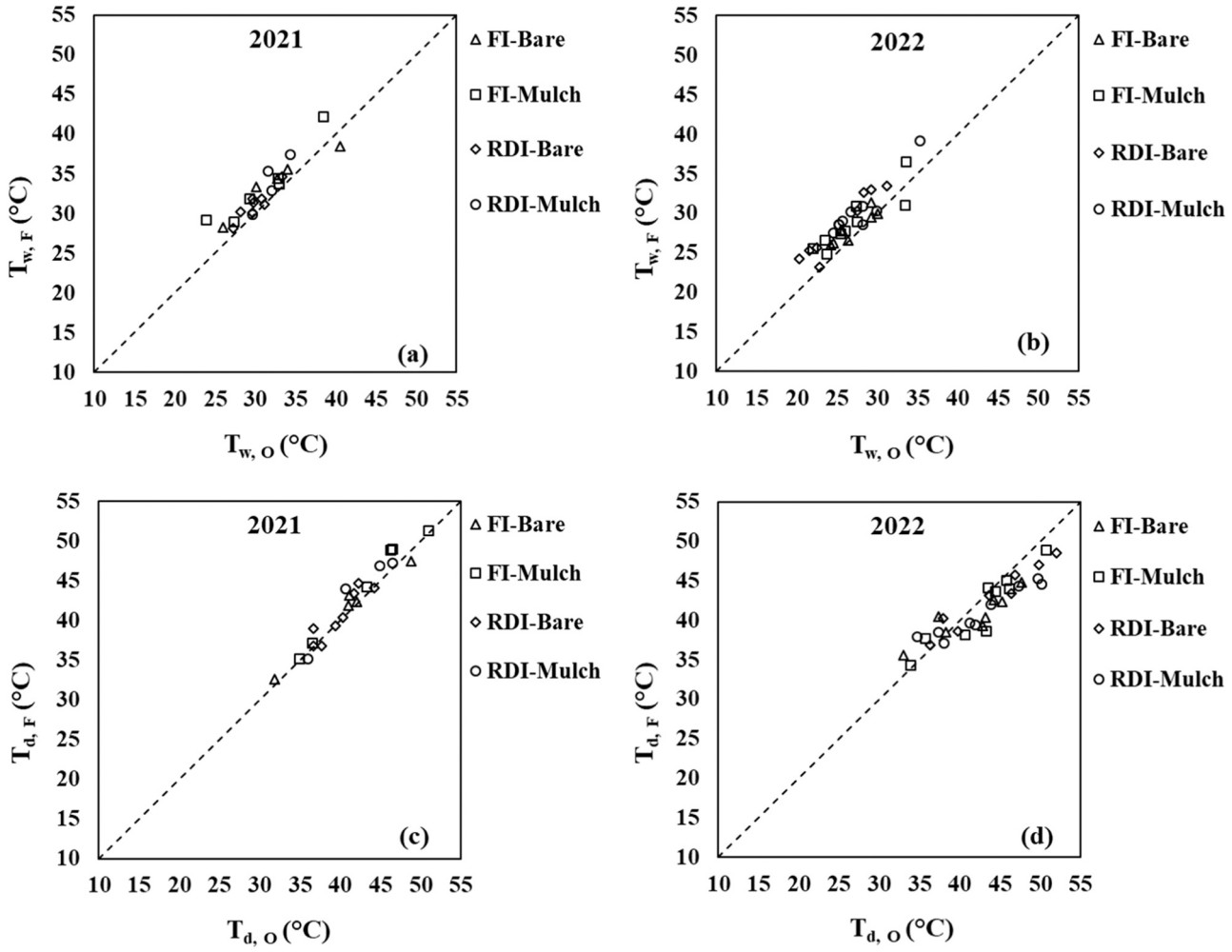

Fig. 5. Comparison between leaf temperature data for both sensors (Optris Xi 400, O; and FLIR One Pro, F) for all dates and trees in the different treatments in 2021 and 2022: wet leaf temperature (T_w) in (a) 2021 and (b) 2022; and dry leaf temperature (T_d) in (c) 2021 and (d) 2022.

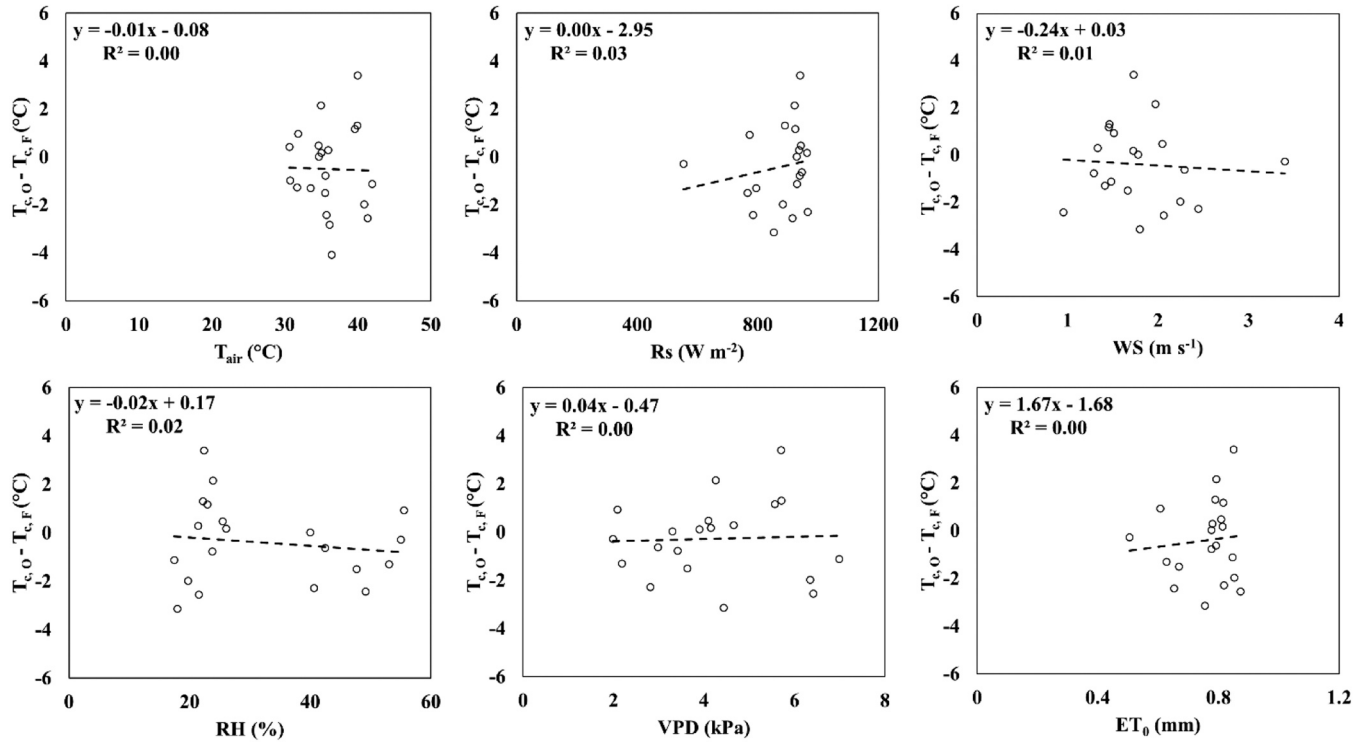

Fig. 6. Correlation between the agrometeorological variables and the canopy temperature (T_c) difference between Optris Xi 400 (O) and FLIR One Pro (F) sensors. T_a, R_s, WS, RH, VPD and ET_0 refer to air temperature, solar radiation, relative humidity, vapor pressure deficit and reference evapotranspiration, respectively.

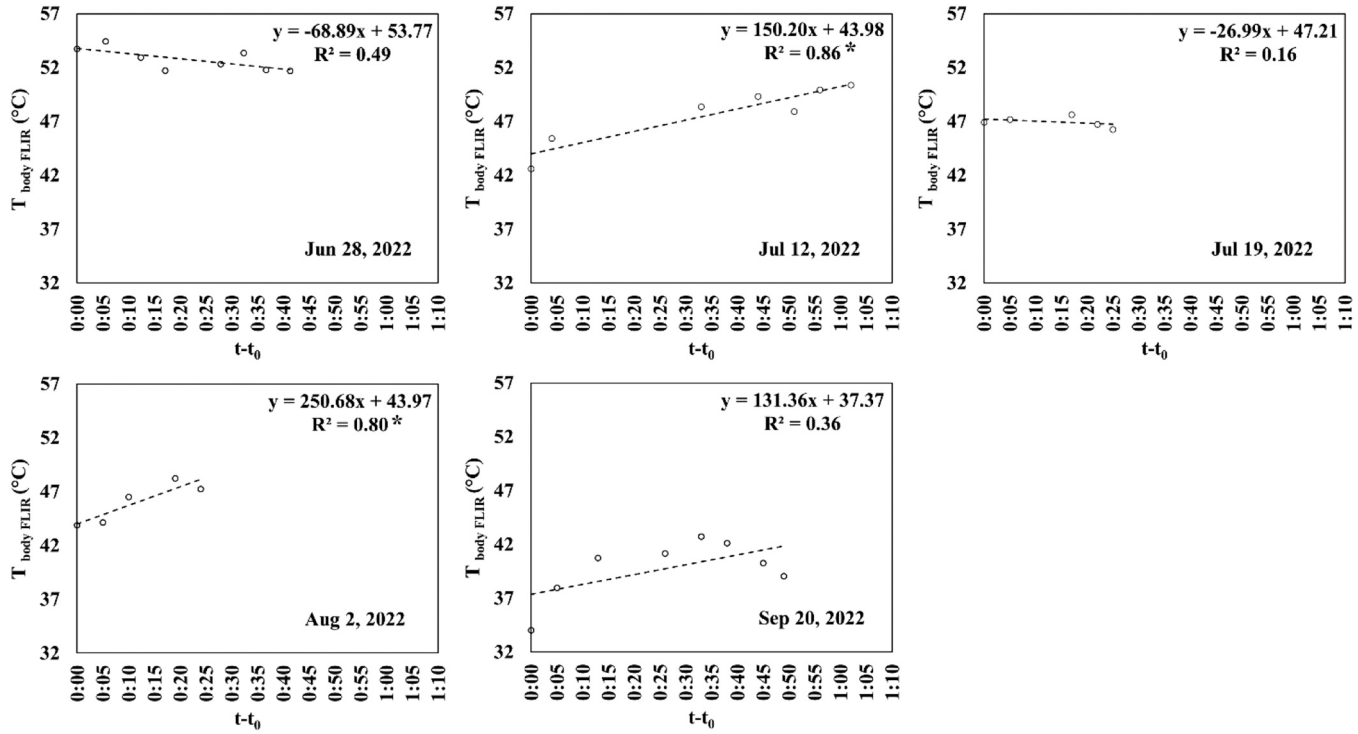

Fig. 7. Correlation between body FLIR temperature ($T_{body\ FLIR}$) and acquisition duration ($t\text{-}t_0$) for each acquisition campaign. Asterisks indicate significant relationships at p value ≤ 0.05.

main actions (Fig. 3): (i) conversion of the raw data into csv files using the FLIR Tools software (Teledyne FLIR LLC, Arlington, Virginia) and Optris PIX Connect (Optris GmbH, Berlin, Germany); (ii) conversion of the cvs into tiff format images using a toolbox specifically created in ArcGIS software (v. 10.5; Esri, Redlands, CA, USA); (iii) manually referencing the FLIR images to ensure the overlapping with the Optris images (Fig. 2); (iv) emissivity (ε) correction of the FLIR images, assuming a value of 0.98 for the tree canopy emissivity (Apogee Instruments, Inc, 2020); (v) identification and digitalization of dry and wet leaves and extraction of their temperatures (T_w and T_d) (Fig. 2); and (iv)

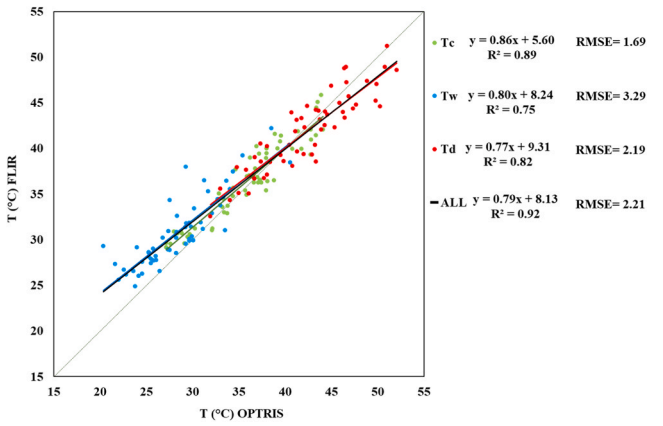

Fig. 8. Correlation of canopy temperature (T_c), wet (T_w) and dry (T_d) leaves between the two sensors (Optris Xi 400 and FLIR One Pro) for all treatments and years.

statistical comparison between the temperature provided by the different sensors (Fig. 2). Outliers leaves temperature measurements (i.e. not included between T_w and T_d) were discarded from the analysis.

Finally, the influence of weather conditions on sensor sensitivity was evaluated through the correlation between the main agrometeorological variables (Table 2) and the difference in T_c between the Optris and FLIR sensors (see "3.2 Influence of meteorological conditions on sensor sensitivity and sensor body temperature").

2.3. Physiological data acquisition

Plant water status was monitored, during the same dates as for thermal data acquisition (Table 2), by measuring Ψ_{stem} with a portable Scholander pressure chamber (Model 3115, Soilmoisture equipment corp., Santa Barbara, CA, USA). Measurements were performed at midday on 2 fully exposed sunlit mature leaves (Corell González et al., 2020) per sample tree. Leaves were covered with aluminum foil for at least one hour prior to measurements, and once cut, they were placed immediately in the pressure chamber with the petiole exposed and pressurized with nitrogen.

2.4. Statistical analysis

The performance of the FLIR sensor was evaluated with respect to the Optris camera by evaluating the slope and intercept values of the regression line, the coefficient of determination (R^2) the root-mean-square error (RMSE, °C; Eq. 2) and the percent of BIAS (PBIAS, %; Eq. 3).

$$\mathrm{RMSE} = \sqrt{\frac{\sum_{i=1}^{n}\left(T_{c,O} - \mathrm{T_{c,F}}\right)^2}{\mathrm{n}}} \quad (2)$$

$$\mathrm{PBIAS} = 100 * \frac{\sum_{i=1}^{n}(T_{c,O} - \mathrm{T_{c,F}})}{\sum_{i=1}^{n} T_{c,O}} \quad (3)$$

where n is the number of observations, $T_{c,O}$ and $T_{c,\ F}$ are the canopy temperatures values obtained from Optris and FLIR sensors, respectively.

For assessing CWSI differences between treatments and sensors, a multi-factorial analysis of variance (ANOVA) per date was performed using Statistix software (v.9.0, Analytical Software 2105 Miller Landing Rd Tallahassee, FL 32312). The same software was also used to perform, for each date, a one-way ANOVA on the Ψ_{stem} values of each treatment for identifying statistical differences in the physiological status. When significant differences were identified (between treatments, sensors or the treatment-sensor interaction), a mean comparison test using Tukey's honest significant difference method was performed, with the 95% of confidence level (p-value < 0.05). Finally, the relationship existent between Ψ_{stem} and T_c-T_a and CWSI, respectively, were explored analyzing linear regression models (R^2 and trend line equation).

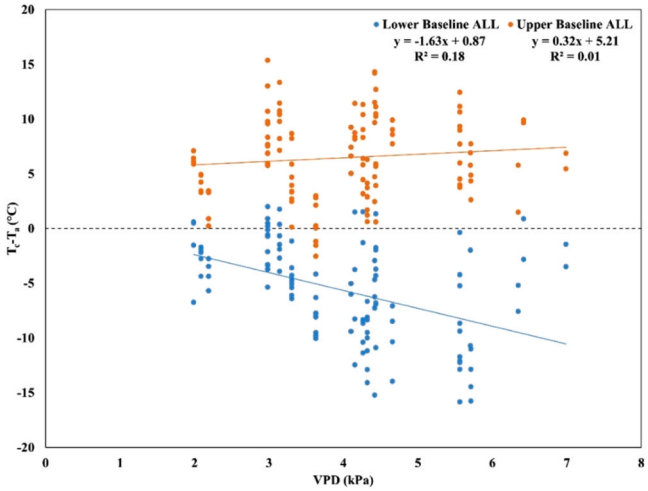

Fig. 10. Difference between canopy temperature (T_c) obtained from Optris Xi 400 and FLIR One Pro together; and air temperature (T_a) as a function of observed vapor pressure deficit (VPD) for all treatments and years.

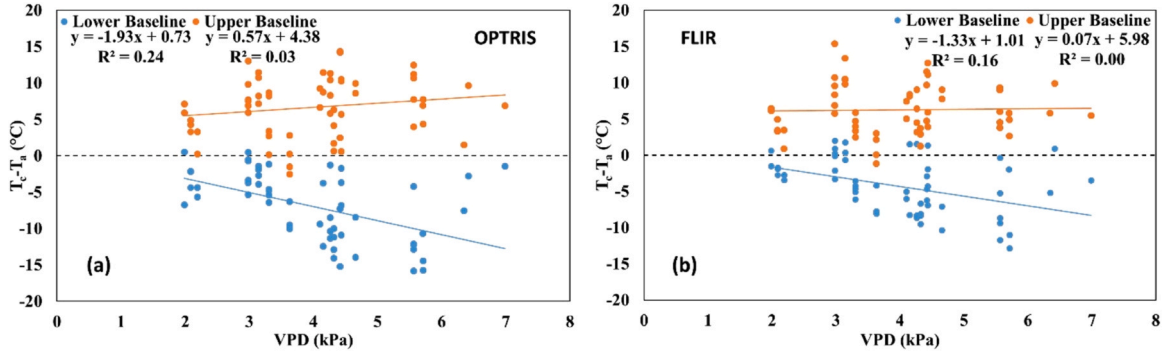

Fig. 9. Difference between canopy temperature (T_c) obtained from (a) Optris Xi 400 and (b) FLIR One Pro; and air temperature (T_a) as a function of observed Vapor Pressure Deficit (VPD) for all treatments and years.

Table 5
Wet (T_w) and dry (T_d) temperatures and standard error (SE) acquired with Optris Xi 400 and FLIR One Pro, used for each specific date.

Date	Leaf	Temperature (°C)	SE (°C)
Jul 22, 2021	$T_{w\ Optris}$	28.19	0.57
	$T_{d\ Optris}$	46.57	0.73
	$T_{w\ FLIR}$	30.24	0.52
	$T_{d\ FLIR}$	48.92	0.89
Jul 29, 2021	$T_{w\ Optris}$	33.31	2.15
	$T_{d\ Optris}$	50.99	2.59
	$T_{w\ FLIR}$	35.68	1.90
	$T_{d\ FLIR}$	51.23	1.42
Aug 24, 2021	$T_{w\ Optris}$	25.22	2.02
	$T_{d\ Optris}$	46.60	2.32
	$T_{w\ FLIR}$	31.81	1.77
	$T_{d\ FLIR}$	48.82	2.06
Sep 1, 2021	$T_{w\ Optris}$	23.96	3.57
	$T_{d\ Optris}$	37.72	0.56
	$T_{w\ FLIR}$	26.71	1.01
	$T_{d\ FLIR}$	37.14	0.20
Sep 21, 2021	$T_{w\ Optris}$	26.00	0.90
	$T_{d\ Optris}$	36.67	1.06
	$T_{w\ FLIR}$	28.22	0.44
	$T_{d\ FLIR}$	36.73	0.86
Jun 28, 2022	$T_{w\ Optris}$	23.78	1.30
	$T_{d\ Optris}$	52.06	1.07
	$T_{w\ FLIR}$	30.91	1.63
	$T_{d\ FLIR}$	48.94	0.81
Jul 12, 2022	$T_{w\ Optris}$	22.53	1.37
	$T_{d\ Optris}$	46.41	0.75
	$T_{w\ FLIR}$	26.28	1.54
	$T_{d\ FLIR}$	43.36	0.75
Jul 19, 2022	$T_{w\ Optris}$	27.12	0.89
	$T_{d\ Optris}$	43.32	1.66
	$T_{w\ FLIR}$	28.54	0.42
	$T_{d\ FLIR}$	41.52	0.58
Aug 2, 2022	$T_{w\ Optris}$	20.33	1.70
	$T_{d\ Optris}$	49.88	2.17
	$T_{w\ FLIR}$	27.61	1.17
	$T_{d\ FLIR}$	47.07	1.13
Sep 20, 2022	$T_{w\ Optris}$	21.61	0.81
	$T_{d\ Optris}$	41.98	1.05
	$T_{w\ FLIR}$	26.20	0.54
	$T_{d\ FLIR}$	39.41	0.61

3. Results

3.1. Performance assessment of low-cost sensor

Fig. 4 shows the comparison between T_c values obtained from FLIR ($T_{c,F}$) and Optris ($T_{c,O}$) sensors for the different treatments applied at the study area, during the years 2021 and 2022. The main statistical metrics (i.e., a, b, R^2, RMSE and PBIAS) are given in Table 4. The same comparison in terms of T_w and T_d is reported in Fig. 5 and Table 4.

A general good agreement was observed between T_c obtained from the two sensors (Fig. 4), existing a significant relationship among them for all evaluated dates (Table 4). Specifically, slope and intercepts terms vary from 0.68 to 1.38 and from 1.91 to 12.50 ºC, respectively. Moreover, R^2 values ranged from 0.93 to 0.99 and from 0.93 to 0.97 in 2021 and 2022, respectively; RMSE values ranged from 1.77° to 2.24°C and from 1.47° to 2.10°C for the years 2021 and 2022, respectively (Table 4). FLIR sensor overestimated $T_{c,O}$ for all the treatments and years, with PBIAS values ranging from − 2.52% to − 4.39% and from − 0.95–1.85% for the years 2021–2022, respectively (Table 4).

Regarding T_w and T_d, significant relationships between the values provided by FLIR and Optris sensors were obtained in all dates (Table 4). A clear pattern was also observed when comparing T_w and T_d during both irrigation season, with T_d presenting higher values (≈ 32–53 ºC) than T_w (≈ 20–41 ºC) (Fig. 5). The obtained relationships were close to the 1:1 line, with slope terms varying from 0.68 to 1.53 and from 0.52 to 1.14 for T_w and T_d, respectively; and intercept values ranging from 2.92 to 14.94 ºC and from 0.87 to 18.98 ºC for T_w and T_d, respectively (Table 4). During the year 2021, R^2 values for T_w and T_d relationships ranged from 0.84 to 0.93 and from 0.84 to 0.98, respectively, with RMSE values varying from 1.42° to 2.98°C and from 1.16° to 1.97°C, respectively. The PBIAS values showed that T_w and T_d obtained with FLIR sensor overestimated the temperature values obtained from Optris sensor for all the treatments, with values ranging from − 4.11 to − 8.36% and from − 1.07 to − 2.58% for the T_w and T_d, respectively.

During the year 2022, R^2 values varied from 0.80 to 0.91 and from 0.80 to 0.94 for T_w and T_d, respectively, with RMSE values ranging from 1.63° to 3.28°C and from 2.16° to 3.09°C for T_w and T_d, respectively. Overestimations were observed for T_w values ranging from − 4.95 to − 12.05%, while for T_d, FLIR sensor underestimated Optris temperatures (PBIAS from 2.41% to 4.07%).

3.2. Influence of meteorological conditions on sensor sensitivity and sensor body temperature

Fig. 6 shows the correlations between the T_c difference between the two sensors ($T_{c,\ O}$ - $T_{c,\ F}$) and the agrometeorological variables monitored at the study area (T_a, Rs, WS, RH, VPD, ET_0, Table 2). $T_{c,\ O}$ - $T_{c,\ F}$ were weakly (R^2 values ≤ 0.03) and not significantly (p-values > 0.05) correlated with respect to the agrometeorological variations in terms of T_a, R_s, WS, RH, VPD, and ET_0 (Fig. 6). This lack of significance was also evident from the close to 0 slope terms (−0.02 to 1.67) and the nearly horizontal pattern (Fig. 6).

Fig. 7 shows the correlation between the temperature trend of the FLIR sensor body ($T_{body\ FLIR}$) with the acquisition duration from the first to the last monitored tree ($t\text{-}t_0$) for DOYs 179, 193, 200, 214 and 263.

In general terms, the variation in $T_{body\ FLIR}$ with time was not constant for all dates, observing that it warmed between 4 and 8 ºC in three out the five assessed dates (July 12, August 2 and September 20), while it kept almost invariable in the other two dates ($T_{body\ FLIR}$ variations with time lower than 2 ºC; June 28 and July 19). Moreover, only in two of the five dates a significant correlation was found with R^2 values ranging from 0.80 to 0.86 showing that $T_{body\ FLIR}$ increases significantly over time, while in the remaining dates no significant relationship was observed between the $T_{body\ FLIR}$ and the acquisition time with, R^2 values ranged from 0.16 to 0.49 (Fig. 7).

3.3. Assessment of the CWSI from FLIR sensor versus Optris sensor as indicator of tree water stress

Fig. 8 shows the correlation between T_c, T_w and T_d obtained from the two sensors for all treatments and years under study. The individual correlations obtained for T_c, T_w and T_d had slope and intercept values of 0.77–0.86, and 5.60–9.31 ºC, respectively, with high accuracy in terms of R^2 and RMSE (0.75–0.89 and 1.69–3.29 ºC, respectively; Fig. 8). The global relationship obtained when considering all the data together showed slope, intercept, R^2 and RMSE values of 0.79, 8.13 ºC, 0.92 and 2.21 ºC, respectively (Fig. 8). The best agreement between both sensors (i.e., where the regression lines cross the 1:1 line) occurred at temperatures of about 41ºC (Fig. 8).

The upper and lower baselines derived from T_w and T_d, derived from Optris and FLIR sensors are represented in Figs. 9 and 10, respectively. For the upper baselines obtained from the two sensors (i.e., Fig. 9), both of them were nearly constant (i.e. independent on VPD) at values of 6 and 7 ºC for FLIR and Optris, respectively. Regarding the lower baselines, their slope and intercept values varied from − 1.93 to − 1.33 and from 0.73 to 1.01 ºC, respectively; depending on the sensor utilized. When plotting the baselines from both sensors together, a general upper baseline of $(T_c\text{-}T_a)_{UL}$= 7 ºC and a lower baseline of $(T_c\text{-}T_a)_{LL}$= −1.63 *VPD+ 0.87, were obtained. However, a high dispersion was observed in the baselines, as evidenced by their low R^2 values (Figs. 9 and 10).

Table 5 summarizes the values of T_w and T_d obtained for each date from the different sensors.

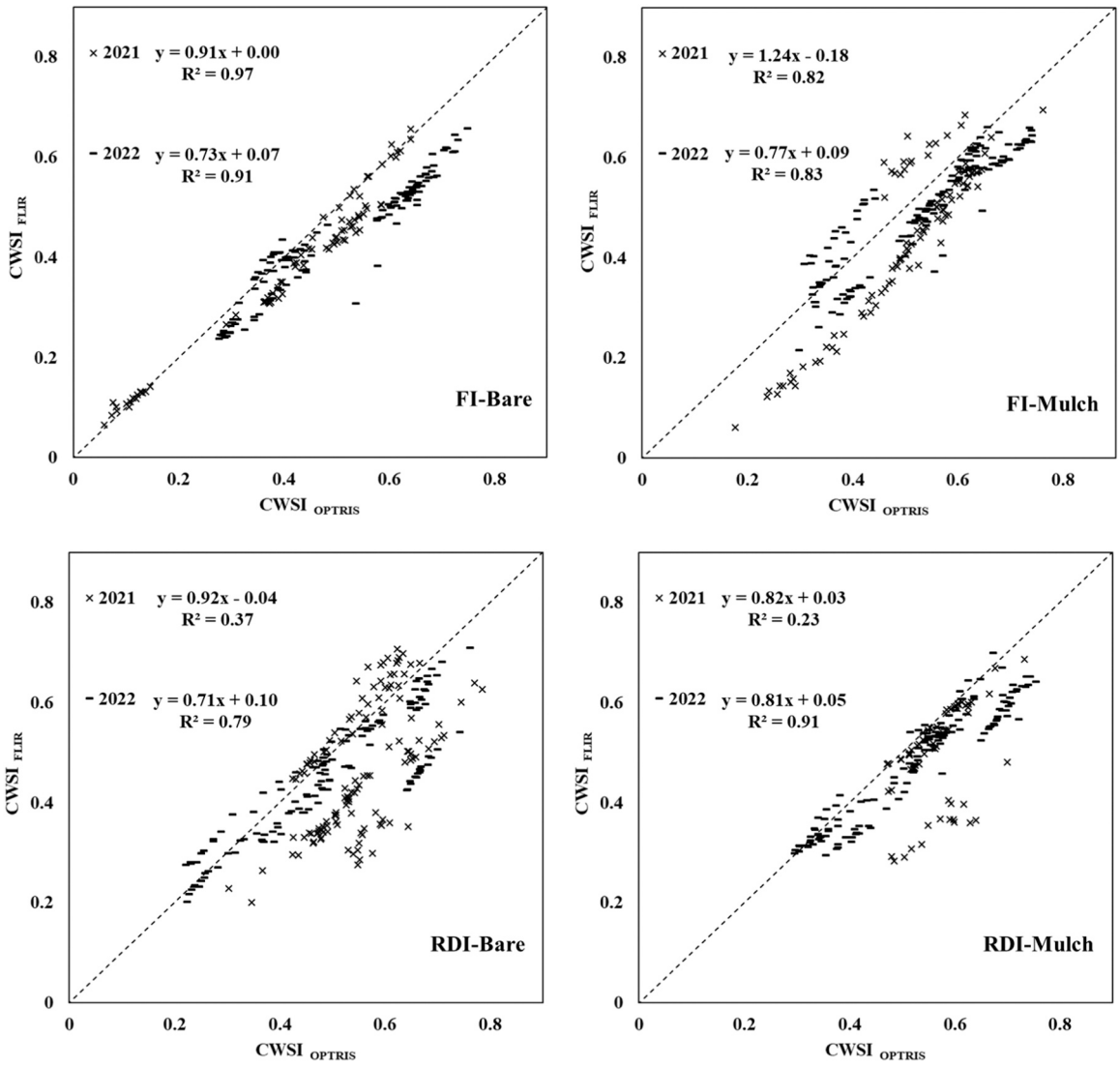

Fig. 11. Relationship between crop water stress index (CWSI) calculated with FLIR One Pro and Optris Xi 400 sensors for each treatment and year.

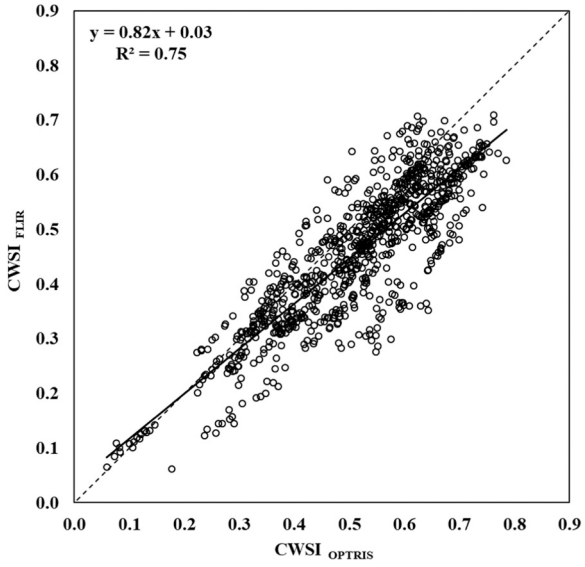

Fig. 12. Relationship between the crop water stress index (CWSI) calculated with FLIR One Pro and Optris Xi 400 sensors for all treatments and years.

An average difference of around 4.02 ºC was obtained when comparing $T_{w\ Optris}$ and $T_{w\ FLIR}$, observing some dates with a high agreement among T_w provided by both sensors (differences of around 2.00ºC; July 22, 2021; and July 19, 2022) (Table 5); and other dates when the differences between T_w provided by both sensors exceeded 7.00 ºC (June 28 and August 2, 2022; Table 5). A better response was obtained in terms of T_d, with mean differences among sensors of 1.88 ºC, with only two dates presenting T_d differences among sensors higher than 3.00 ºC (June 28 and July 12, 2022; Table 5). Regarding the SE values, most T_w and T_d measurements presented SE values lower than 2.00 ºC, with only one data presenting a SE value higher than 3.00ºC (SE of 3.57 ºC for $T_{w\ Optris}$ on September 1, 2021; Table 5).

Figs. 11 and 12 show the comparison between the CWSI determined from FLIR and Optris sensors for the different treatments and considering all of them together, respectively. In general, a good agreement between the calculated CWSI values was observed for all the treatments, with R^2 and RMSE values ranging from 0.79 to 0.97 and 0.05–0.06 respectively, with the exception of RDI-Bare and RDI-Mulch in 2021, where a lower performance was obtained (R^2 lower than 0.40 and RMSE values of 0.11–0.13).

Absolute CWSI values varied from 0.05 to 0.80 during the irrigation seasons. Additionally, CWSI derived from Optris and FLIR sensors resulted statistically different in almost all the evaluated dates, being

Table 6
Average and standard error (SE) of the CWSI obtained from Optris Xi 400 and FLIR One Pro sensors. Different letters identify, for each date, significant differences among treatments and sensors ($p \leq 0.05$). Asterisk indicates not significance in the interaction "Treatment × Sensor", identifying in those cases differences among sensors using lowercase and uppercase letters. Empty cells correspond to leaves discarded due to incorrect establishment of wet and dry conditions.

Date	Treatment	$CWSI_{Optris}$		$CWSI_{FLIR}$	
		Average	SE	Average	SE
Jul 22, 2021 *	FI-Bare	0.50B	0.01	0.44b	0.01
	FI-Mulch	0.60 A	0.01	0.54a	0.01
	RDI-Bare	0.50B	0.01	0.45b	0.02
	RDI-Mulch	0.58 A	0.01	0.56a	0.01
Jul 29, 2021	FI-Bare	0.57b	0.01	0.57b	0.02
	FI-Mulch	0.52c	0.01	0.60b	0.01
	RDI-Bare	0.60b	0.01	0.65a	0.01
	RDI-Mulch	-	-	-	-
Aug 24, 2021	FI-Bare	0.39e	0.01	0.35 f	0.01
	FI-Mulch	0.51bc	0.01	0.42de	0.01
	RDI-Bare	0.56a	0.01	0.45d	0.01
	RDI-Mulch	0.55ab	0.01	0.50c	0.01
Sep 1, 2021 *	FI-Bare	-	-	-	-
	FI-Mulch	0.46B	0.01	0.33b	0.02
	RDI-Bare	0.69 A	0.01	0.53a	0.01
	RDI-Mulch	-	-	-	-
Sep 21, 2021	FI-Bare	0.11e	0.01	0.11e	0.01
	FI-Mulch	0.29c	0.01	0.16d	0.01
	RDI-Bare	0.57a	0.01	0.33bc	0.01
	RDI-Mulch	0.58a	0.01	0.36b	0.01
Jun 28, 2022	FI-Bare	0.62c	0.01	0.50e	0.01
	FI-Mulch	0.66b	0.01	0.60c	0.01
	RDI-Bare	0.67ab	0.00	0.54d	0.01
	RDI-Mulch	0.70a	0.01	0.59c	0.01
Jul 12, 2022	FI-Bare	0.67a	0.01	0.56bcd	0.01
	FI-Mulch	0.65a	0.01	0.59b	0.01
	RDI-Bare	0.55 cd	0.01	0.54d	0.01
	RDI-Mulch	0.58bc	0.01	0.57bcd	0.01
Jul 19, 2022	FI-Bare	0.39c	0.01	0.40c	0.01
	FI-Mulch	0.38c	0.01	0.46ab	0.01
	RDI-Bare	-	-	-	-
	RDI-Mulch	0.47a	0.01	0.42bc	0.02
Aug 2, 2022 *	FI-Bare	-	-	-	-
	FI-Mulch	0.54 A	0.00	0.48a	0.01
	RDI-Bare	0.45B	0.01	0.40b	0.01
	RDI-Mulch	0.53 A	0.01	0.48a	0.01
Sep 20, 2022	FI-Bare	0.34ab	0.01	0.29c	0.01
	FI-Mulch	0.37a	0.01	0.34ab	0.01
	RDI-Bare	0.29c	0.01	0.31bc	0.01
	RDI-Mulch	0.34ab	0.01	0.34ab	0.01

those derived from Optris higher than those from FLIR (Table 6).

When analyzing the relative effects of the soil management on the CWSI, bare treatments (average CWSI of 0.50 and 0.44 for Optris and FLIR sensors, respectively) exhibited significantly lower or equal CWSI values than those corresponding with Mulch treatments (average CWSI of 0.52 and 0.46 for Optris and FLIR sensors, respectively), both under FI and RDI conditions (except for Optris in July 29, 2021 under FI conditions) (Table 6). Regarding the irrigation strategies, average CWSI for FI treatments during the irrigation seasons varied from 0.40 to 0.50; whereas average CWSI for RDI treatments reached values of 0.46–0.55. CWSI values calculated for each irrigation treatment from Optris and FLIR sensors identified the same patterns, although this trend was not constant during the entire study period. Specifically, FI treatments presented significantly lower CWSI values than RDI treatments on 21 September 2021 and 28 June 2022; and significantly higher CWSI values than RDI treatments on 12 July and 20 September 2022 (Table 6). However, there were some specific dates when exceptions occurred, as on 24 August and 29 June 2021, when Optris and FLIR-derived CWSI trends for the different irrigation strategies differed both under bare soil and mulching conditions (i.e., Optris identified differences among FI and RDI treatments but FLIR did not, or viceversa; Table 6). Especially relevant was the lack of statistical differences among the irrigation treatments under mulching conditions using FLIR sensor in 2022 (Table 6).

3.4. Relationship between steam water potential and thermal parameters

Physiological measurements taken during the entire study period showed that tree Ψ_{stem} for all evaluated treatments ranged from − 1.0 to − 2.5 MPa. Figs. 13–15 represent the relationship between T_c-T_a and Ψ_{stem} and between CWSI and Ψ_{stem}.

These relationships were assessed individually for each single treatment (Figs. 13 and 14), and considering all treatments together (Fig. 15). No relationships between the evaluated variables (T_c-T_a vs Ψ_{stem} and CWSI vs Ψ_{stem}) were obtained, as represented by the low R^2 values achieved (lower than 0.3 in all the cases).

4. Discussion

Despite infrared thermal sensing has been demonstrated as a useful tool for monitoring crop water stress, only few studies have evaluated the performance of low-cost sensors in comparison with professional ones (García-Tejero et al., 2018; Noguera et al., 2020; Giménez-Gallego et al., 2021; Irsyad et al., 2022; Carrasco-Benavides et al., 2020). This kind of studies are necessary in order to evaluate if the reduction in the cost of the sensors, and therefore, of the data quality provided by them (e.g. sensor specifications in Table 3), are acceptable for crop water status monitoring. In this regard, the low-cost sensor used in the present study provided accurate T_c measurements when compared with a professional sensor, with RMSE values lower than 2.5ºC. This accuracy is in line with the accuracies provided by most of the commercial thermal sensors, generally with values of less than ± 2ºC (e.g., low or medium-cost sensors from FLIR, Fluke and Optris manufacturers).

Several authors have evidenced the influence that agrometeorological conditions have on the thermal signal (Maes et al., 2017; Petrie et al., 2019; Ramírez-Cuesta et al., 2022b). These agrometeorological conditions can modify the temperature of the sensor, body and lens (especially on most of the low-cost sensors as they are uncooled microbolometer sensors); and also affect temperature measurements due to the attenuation of the thermal radiance by the atmosphere (Maes et al., 2017). Among the agrometeorological variables, WS has been identified as one of the strongest contributor to surface temperature measurement uncertainty (Yamada et al., 1996; Lehmann et al., 2013; Petrie et al., 2019). However, in our study, the agrometeorological conditions occurred during the field campaigns did not seem to affect the differences observed in the temperature values registered by the Optris and FLIR sensors (Fig. 6). The absence of agrometeorological effects on T_c measurements could be related to the fact that sensor was kept under homogeneous shade conditions except for the image acquisition moment; whereas other authors intentionally included some meteorological challenging conditions in their studies (Petrie et al., 2019; Ramírez-Cuesta et al., 2022b). These results evidence the necessity of ensuring homogeneous meteorological conditions in order to not affect the accuracy of the low-cost sensors.

However, the accuracies provided by thermal sensors are subject to some limitations for identifying crop water stress, especially at low VPD values (i.e., lower than 2 kPa), when the upper and lower baselines are closer to each other. In this way, a small error in T_c determination could result in high inaccuracies of CWSI (Gonzalez-Dugo and Zarco-Tejada, 2022). Nonetheless, from an agronomic point of view, this limitation is not especially relevant, since the greatest interest and applicability of the CWSI occurs at high crop water demands conditions (i.e., high VPD values). Determining crop water status becomes even more difficult when integrating data acquired in different dates, since T_c has been demonstrated to vary rapidly with changes in the agrometeorological and environmental conditions (Ramírez-Cuesta et al., 2022b); which makes the definition of the baselines a complex procedure, as represented by the high dispersion observed in Figs. 9 and 10.

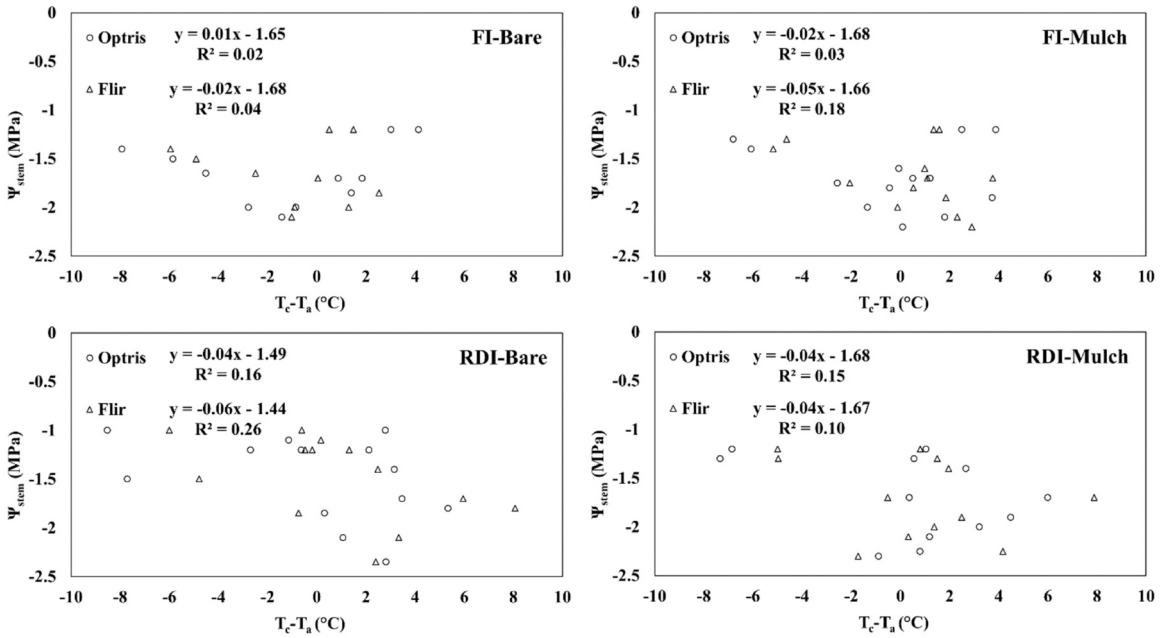

Fig. 13. Relationship between midday stem water potential (Ψ_{stem}) and the difference between canopy (T_c) and air temperature (T_a), determined for each individual treatment and for all years.

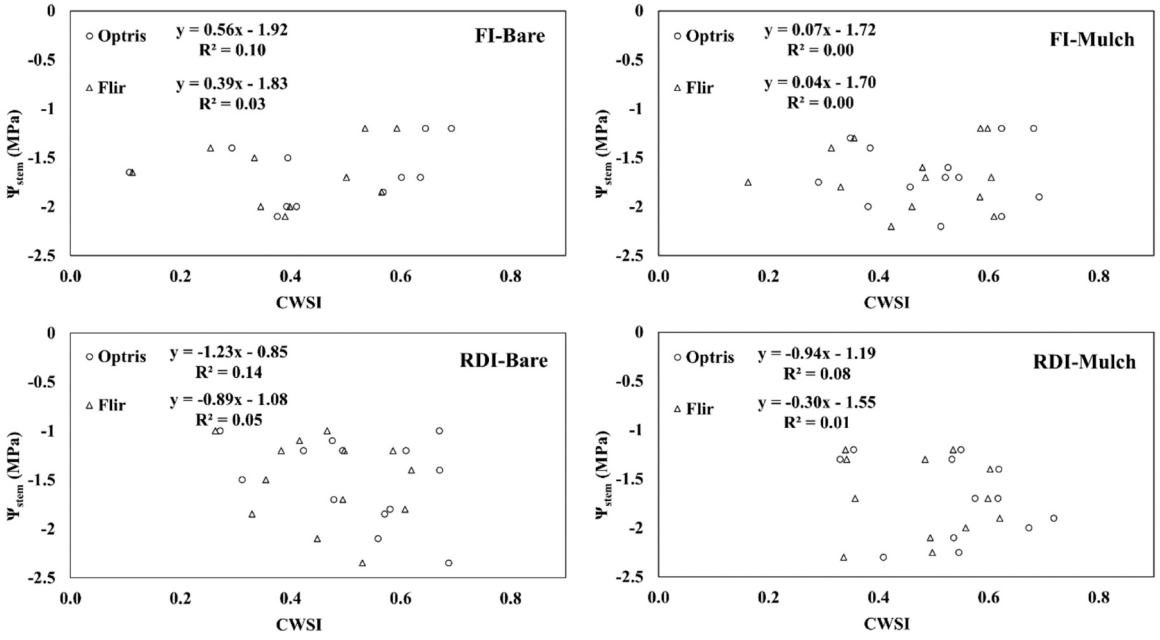

Fig. 14. Relationship between midday stem water potential (Ψ_{stem}) and crop water stress index (CWSI) determined for each individual treatment and for all years.

Determining the baselines is not an easy task and proof of that is the variability in the lower baselines obtained for citrus in literature. In this sense, Gonzalez-Dugo et al. (2014) obtained lower limits equal to $-0.38 \times VPD + 4.59$ and to $-0.50 \times VPD + 4.06$ for orange and mandarin orchards at Seville (Spain), respectively; whereas Jamshidi et al. (2021) obtained a similar lower limit of $-0.57 \times VPD + 2.31$ for an orange orchard in Iran. Also for orange, Barbagallo et al. (2009) found a lower limit of $-2.34 \times VPD + 0.91$ in an area located close to the experimental site of our study (Sicily, Italy). Moreover, Sepaskhah and Kashefipour (1994) established their lower baseline as $-1.74 \times VPD + 3.61$ for sweet lime in Iran; whereas for lemon, Waldo and Schumann (2009) identified in Florida (USA) a lower baseline equal to $-1.83 \times VPD + 9.47$. Such baselines variability was already evidenced by Gonzalez-Dugo et al. (2014) who observed more scattering in the lower limit of citrus than on other tree crops, attributing such differences to fluctuations in T_c, stomatal resistance and canopy conductance.

Other sources of uncertainty in the lower baseline establishment are the crop load, the position in the tree canopy where the thermal measurement is performed, the water use and transpiration of each species, and the age of the leaves, among others (Gonzalez-Dugo et al., 2014; Gonzalez-Dugo and Zarco-Tejada, 2022; Ramírez-Cuesta et al., 2022a). This variability makes difficult the possibility of transferring a site-specific baseline to other study sites without a prior verification of the appropriateness of these baselines. For this reason, it might be advisable to use, as an alternative to general theoretical or empirical

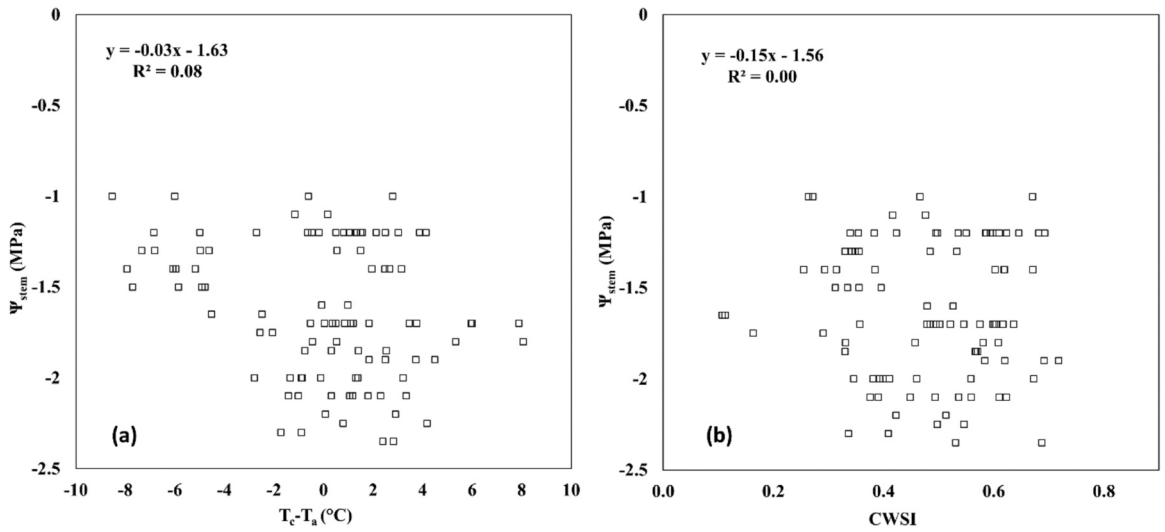

Fig. 15. Relationship between midday stem water potential (Ψ_{stem}) and the difference between canopy (T_c) and air temperature (T_a) (a) and crop water stress index (CWSI) (b) determined for all treatments and years.

baselines, wet and dry references taken in the same photograph of the leaf to be analyzed, to verify that their temperatures have been recorded under the same meteorological temperature and environmental conditions. This approach relies more in the relative T_c values in comparison to T_w and T_d than in the T_c absolute values. Thus, the thermal sensitivity of the sensors (80 and 150 mK for FLIR One Pro and Optris Xi 400, respectively; Table 3) would play a more critical role than the sensor absolute accuracy ($\pm$ 3 and $\pm$ 2 ºC for FLIR One Pro and Optris Xi 400, respectively; Table 3). This proposed approach is in line with the main idea of the CWSI concept, i.e., identify how far or how close is the leaf of interest from the anchor conditions.

The establishment of wet and dry conditions on the leaves (i.e., T_w and T_d) resulted also a critical step, as evidenced by high variability observed in T_w and T_d values during each measurement campaign (SE between dates of 0.20–3.57 ºC; Table 5). It highlights that the proper establishment of wet and dry conditions can be more critical than the use of one or another sensor. In this sense, special attention needs to be paid to not take the photograph when the wet leaf has still water on the surface, since it could result in an underestimation of the T_w, and subsequently, in an overestimation of the CWSI. Similarly, petroleum jelly needs to be homogeneously applied to avoid transpiring areas that could diminish the leaf temperature, thus underestimating T_d and again resulting in a CWSI overestimation.

Finally, clear relationships between T_c-T_a and Ψ_{stem}; and between CWSI and Ψ_{stem} were not observed in the present study. It could reflect the isohydric behavior of most citrus species (Pérez-Pérez et al., 2012; Romero-Trigueros et al., 2021), which close stomata when they feel an increase in the atmospheric demand, regulating transpiration water loss and minimizing fluctuations in water potential. These results may evidence a potential limitation of the use of midday Ψ_{stem} as a crop water stress indicator, mainly related to the time of the measurements acquisition, since at midday, citrus could have the stomata completely closed (i.e. similar Ψ_{stem} values) independently on the irrigation strategy. In this sense, other authors have evidenced that alternative measurements performed early in the morning (before citrus stomata closure), such as the pre-dawn water potential, gas exchange and chlorophyll fluorescence parameters are able to identify citrus water status of trees under different watering regimes (Pérez-Pérez et al., 2016; Santana-Vieira et al., 2016; Romero-Trigueros et al., 2021).

5. Conclusion

The main results of this study show good reliability and accuracy of the FLIR One Pro sensor, in defining the T_c, T_w and T_d, without being these temperatures influenced by the agrometeorological conditions. Even if, no overheating of the low-cost sensor was observed during the experiment, it is advisable to keep it under homogeneous weather conditions during the acquisition process (e.g., sensor placed in the shade).

The study reports good correlation for the calculation of the CWSI with both the sensors under evaluation (low-cost versus professional sensors), highlighting the sensitivity of the CWSI calculation (i.e., over- or underestimates) due to the uncertainties related to the identification of the upper and lower baselines (i.e., T_w and T_d). In this sense, this study recommends to use the T_w and T_d thresholds directly derived from the photogram, rather than using empirical references baselines, implementing a rigorous protocol for their identification (e.g., drying the leaf wet and evenly distribute the vaseline in the dry leaf). As expected, no correlation was found between the CWSI and the T_c-T_a with Ψ_{stem}, due to the isohydric behavior of citrus species.

In conclusion, the promising findings of this study may be further enhanced in the near future due to the technological sensors developments, e.g., integrating the video component of the sensor for quickening the measurements speed and reaching greater coverage, or creating a shield to minimize the influence of the agrometeorological conditions for increasing the sensor's accuracy.

Declaration of Competing Interest

The authors declare that they have no known competing financial interests or personal relationships that could have appeared to influence the work reported in this paper.

Data Availability

The authors are unable or have chosen not to specify which data has been used.

Acknowledgments

This study has been partially funded by European Union (NextGeneration EU), through the MUR-PNRR project SAMOTHRACE (E63C22000900006); the projects PRIMA-HANDYWATER (PCI2021-121940) and E-STRESS (TED2021–131448A-I00) funded by MCIN/AEI/10.13039/501100011033 and by the "European Union NextGenerationEU/PRTR"; and the project DigitalRiego (INNEST/2022/63)

financed by the Agencia Valenciana de la Innovación (AVI) and the European Union (ERDF). J.M.R.-C. acknowledges the postdoctoral financial support received from Juan de la Cierva Spanish Postdoctoral Program (IJC2020-043601-I).

References

Abdulridha, J., Ampatzidis, Y., Ehsani, R., de Castro, A.I., 2018. Evaluating the performance of spectral features and multivariate analysis tools to detect laurel wilt disease and nutritional deficiency in avocado. Comput. Electron. Agric. 155, 203–211.

Allen, R.G., Pereira, L.S., Raes, D., Smith, M.1998. Crop evapotranspiration-Guidelines for computing crop water requirements-FAO Irrigation and drainage paper 56. Fao, Rome, 300(9), D05109.

Alvino, A., Marino, S., 2017. Remote sensing for irrigation of horticultural crops. Horticulturae 3 (2), 40.

Ampatzidis, Y., Partel, V., Meyering, B., Albrecht, U., 2019. Citrus rootstock evaluation utilizing UAV-based remote sensing and artificial intelligence. Comput. Electron. Agric. 164, 104900.

Apogee Instruments, Inc. (2020). Owner's manual. Infrared temperature meter. Models MI-210, MI-220, MI-230, and MI-2H0. Apogee Instruments, Inc. Logan. Utah 84321, USA.

Ballester, C., Jiménez-Bello, M.A., Castel, J.R., Intrigliolo, D.S., 2013. Usefulness of thermography for plant water stress detection in citrus and persimmon trees. Agric. For. Meteorol. 168, 120–129.

Barbagallo, S., Consoli, S., Russo, A., 2009. A one-layer satellite surface energy balance for estimating evapotranspiration rates and crop water stress indexes. Sensors 9 (1), 1–21.

Bellvert, J., Zarco-Tejada, P.J., Girona, J., Fereres, E.J.P.A., 2014. Mapping crop water stress index in a 'Pinot-noir'vineyard: comparing ground measurements with thermal remote sensing imagery from an unmanned aerial vehicle. Precis. Agric. 15 (4), 361–376.

Bendig, J., Bolten, A., Bareth, G., 2012. Introducing a low-cost mini-UAV for thermal-and multispectral-imaging. Int. Arch. Photogramm. Remote Sens. Spat. Inf. Sci. 39, 345–349.

Berni, J.A.J., Zarco-Tejada, P.J., Sepulcre-Cantó, G., Fereres, E., Villalobos, F., 2009. Mapping canopy conductance and CWSI in olive orchards using high resolution thermal remote sensing imagery. Remote Sens. Environ. 113 (11), 2380–2388.

Blaya-Ros, P.J., Blanco, V., Domingo, R., Soto-Valles, F., Torres-Sánchez, R., 2020. Feasibility of low-cost thermal imaging for monitoring water stress in young and mature sweet cherry trees. Appl. Sci. 10 (16), 5461.

Carrasco-Benavides, M., Antunez-Quilobrán, J., Baffico-Hernández, A., Ávila-Sánchez, C., Ortega-Farías, S., Espinoza, S., Gajardo, J., Mora, M., Fuentes, S., 2020. Performance assessment of thermal infrared cameras of different resolutions to estimate tree water status from two cherry cultivars: an alternative to midday stem water potential and stomatal conductance. Sensors 20 (12), 3596.

Clarke, T.R., 1997. An empirical approach for detecting crop water stress using multispectral airborne sensors. Horttechnology 7 (1), 9–16.

Cohen, Y., Alchanatis, V., Meron, M., Saranga, Y., Tsipris, J., 2005. Estimation of leaf water potential by thermal imagery and spatial analysis. J. Exp. Bot. 56 (417), 1843–1852.

Cohen, Y., Alchanatis, V., Saranga, Y., Rosenberg, O., Sela, E., Bosak, A.J.P.A., 2017. Mapping water status based on aerial thermal imagery: comparison of methodologies for upscaling from a single leaf to commercial fields. Precis. Agric. 18 (5), 801–822.

Consoli, S., Papa, R., 2013. Corrected surface energy balance to measure and model the evapotranspiration of irrigated orange orchards in semi-arid Mediterranean conditions. Irrig. Sci. 31 (5), 1159–1171.

Consoli, S., Vanella, D., 2014. Comparison of satellite-based models for estimating evapotranspiration fluxes. J. Hydrol. 513, 475–489.

Consoli, S., Stagno, F., Vanella, D., Boaga, J., Cassiani, G., Roccuzzo, G., 2017. Partial root-zone drying irrigation in orange orchards: effects on water use and crop production characteristics. Eur. J. Agron. 82, 190–202.

Corell González, M., Martín Palomo, M., Girón Moreno, I.F., Andreu Cáceres, L., Galindo Egea, A., Centeno, A., Pérez-López, A., Moriana, A., 2020. Stem water potential-based regulated deficit irrigation scheduling for olive table trees. Agric. Water Manag. 242, 106418.

Costa, J.M., Grant, O.M., Chaves, M.M., 2013. Thermography to explore plant–environment interactions. J. Exp. Bot. 64 (13), 3937–3949.

Fisher, D.K., Kebede, H., 2010. A low-cost microcontroller-based system to monitor crop temperature and water status. Comput. Electron. Agric. 74 (1), 168–173.

García-Tejero, I., Durán-Zuazo, V.H., Arriaga, J., Hernández, A., Vélez, L.M., Muriel-Fernández, J.L., 2012. Approach to assess infrared thermal imaging of almond trees under water-stress conditions. Fruits 67 (6), 463–474.

García-Tejero, I.F., Costa, J.M., Egipto, R., Durán-Zuazo, V.H., Lima, R.S.N., Lopes, C.M., Chaves, M.M., 2016. Thermal data to monitor crop-water status in irrigated Mediterranean viticulture. Agric. Water Manag. 176, 80–90.

García-Tejero, I.F., Hernández, A., Padilla-Díaz, C.M., Diaz-Espejo, A., Fernández, J.E., 2017. Assessing plant water status in a hedgerow olive orchard from thermography at plant level. Agric. Water Manag. 188, 50–60.

García-Tejero, I.F., Ortega-Arévalo, C.J., Iglesias-Contreras, M., Moreno, J.M., Souza, L., Tavira, S.C., Durán-Zuazo, V.H., 2018. Assessing the crop-water status in almond (Prunus dulcis mill.) trees via thermal imaging camera connected to smartphone. Sensors 18 (4), 1050.

Giménez-Gallego, J., González-Teruel, J.D., Soto-Valles, F., Jiménez-Buendía, M., Navarro-Hellín, H., Torres-Sánchez, R., 2021. Intelligent thermal image-based sensor for affordable measurement of crop canopy temperature. Comput. Electron. Agric. 188, 106319.

Giordano, M.R., Malings, C., Pandis, S.N., Presto, A.A., McNeill, V.F., Westervelt, D.M., Beekmann, M., Subramanian, R., 2021. From low-cost sensors to high-quality data: A summary of challenges and best practices for effectively calibrating low-cost particulate matter mass sensors. J. Aerosol Sci. 158, 105833.

Gonzalez-Dugo, V., Zarco-Tejada, P.J., 2022. Assessing the impact of measurement errors in the calculation of CWSI for characterizing the water status of several crop species. Irrig. Sci. 1–13.

Gonzalez-Dugo, V., Zarco-Tejada, P.J., Fereres, E., 2014. Applicability and limitations of using the crop water stress index as an indicator of water deficits in citrus orchards. Agric. For. Meteorol. 198, 94–104.

Grant, O.M., Ochagavía, H., Baluja, J., Diago, M.P., Tardáguila, J., 2016. Thermal imaging to detect spatial and temporal variation in the water status of grapevine (Vitis vinifera L.). J. Hortic. Sci. Biotechnol. 91 (1), 43–54.

Gutiérrez, S., Fernández-Novales, J., Diago, M.P., Iñiguez, R., Tardaguila, J., 2021. Assessing and mapping vineyard water status using a ground mobile thermal imaging platform. Irrig. Sci. 39 (4), 457–468.

Han, M., Zhang, H., DeJonge, K.C., Comas, L.H., Gleason, S., 2018. Comparison of three crop water stress index models with sap flow measurements in maize. Agric. Water Manag. 203, 366–375.

Hillnhütter, C., Mahlein, A.K., Sikora, R.A., Oerke, E.C., 2011. Remote sensing to detect plant stress induced by Heterodera schachtii and Rhizoctonia solani in sugar beet fields. Field Crops Res. 122 (1), 70–77.

Idso, S.B., Jackson, R.D., Pinter Jr, P.J., Reginato, R.J., Hatfield, J.L., 1981. Normalizing the stress-degree-day parameter for environmental variability. Agric. Meteorol. 24, 45–55.

Ihuoma, S.O., Madramootoo, C.A., 2017. Recent advances in crop water stress detection. Comput. Electron. Agric. 141, 267–275.

Irsyad, F., Oue, H., Mon, M.M., 2022. Monitoring responses of NDVI and canopy temperature in a rice field to soil water and meteorological conditions (July). In: IOP Conference Series: Earth and Environmental Science, Vol. 1059. IOP Publishing, 012037 (July).

Jackson, R.D., Idso, S.B., Reginato, R.J., Pinter Jr, P.J., 1981. Canopy temperature as a crop water stress indicator. Water Resour. Res. 17 (4), 1133–1138.

Jamshidi, S., Zand-Parsa, S., Niyogi, D., 2021. Assessing crop water stress index of citrus using in-situ measurements, landsat, and sentinel-2 data. Int. J. Remote Sens. 42 (5), 1893–1916.

Jones, H.G., 2004. Irrigation scheduling: advantages and pitfalls of plant-based methods. J. Exp. Bot. 55 (407), 2427–2436.

Khanal, S., Fulton, J., Shearer, S., 2017. An overview of current and potential applications of thermal remote sensing in precision agriculture. Comput. Electron. Agric. 139, 22–32.

Khorsand, A., Rezaverdinejad, V., Asgarzadeh, H., Majnooni-Heris, A., Rahimi, A., Besharat, S., Sadraddini, A.A., 2021. Linking plant and soil indices for water stress management in black gram. Sci. Rep. 11 (1), 1–19.

King, B.A., Shellie, K.C., Tarkalson, D.D., Levin, A.D., Sharma, V., Bjorneberg, D.L., 2020. Data-driven models for canopy temperature-based irrigation scheduling. Trans. ASABE 63 (5), 1579–1592.

Lehmann, B., Ghazi, W.K., Frank, T., Collado, B.V., Tanner, C., 2013. Effects of Individual Climatic Parameters on the Infrared Thermography of Buildings. Appl. Energy 110, 29–43.

Maes, W.H., Huete, A.R., Steppe, K., 2017. Optimizing the processing of UAV-based thermal imagery. Remote Sens. 9 (5), 476.

Mahajan, G.R., Sahoo, R.N., Pandey, R.N., Gupta, V.K., Kumar, D., 2014.). Using hyperspectral remote sensing techniques to monitor nitrogen, phosphorus, sulphur and potassium in wheat (Triticum aestivum L.). Precis. Agric. 15, 499–522.

Mangus, D.L., Sharda, A., Zhang, N., 2016. Development and evaluation of thermal infrared imaging system for high spatial and temporal resolution crop water stress monitoring of corn within a greenhouse. Comput. Electron. Agric. 121, 149–159.

Meron, M., Tsipris, J., Orlov, V., Alchanatis, V., Cohen, Y., 2010. Crop water stress mapping for site-specific irrigation by thermal imagery and artificial reference surfaces. Precis. Agric. 11 (2), 148–162.

Möller, M., Alchanatis, V., Cohen, Y., Meron, M., Tsipris, J., Naor, A., Ostrovsky, V., Sprintsin, M., Cohen, S., 2007. Use of thermal and visible imagery for estimating crop water status of irrigated grapevine. J. Exp. Bot. 58 (4), 827–838.

Morlin Carneiro, F., Angeli Furlani, C.E., Zerbato, C., Candida de Menezes, P., da Silva Gírio, L.A., Freire de Oliveira, M., 2020. Comparison between vegetation indices for detecting spatial and temporal variabilities in soybean crop using canopy sensors. Precis. Agric. 21, 979–1007.

Motisi, A., Consoli, S., Papa, R., Cammalleri, C., Rossi, F., Minacapilli, M., Rallo, G., 2012. Eddy covariance and sap flow measurement of energy and mass exchanges of woody crops in a Mediterranean environment. Acta Hortic. 951, (121 – 128.

Mwinuka, P.R., Mbilinyi, B.P., Mbungu, W.B., Mourice, S.K., Mahoo, H.F., Schmitter, P., 2021. The feasibility of hand-held thermal and UAV-based multispectral imaging for canopy water status assessment and yield prediction of irrigated African eggplant (*Solanum aethopicum* L). Agric. Water Manag. 245, 106584.

Noguera, M., Millán, B., Pérez-Paredes, J.J., Ponce, J.M., Aquino, A., Andújar, J.M., 2020. A new low-cost device based on thermal infrared sensors for olive tree canopy temperature measurement and water status monitoring. Remote Sens. 12 (4), 723.

Pérez-Pérez, J.G., Dodd, I.C., Botía, P., 2012. Partial rootzone drying increases water-use efficiency of lemon Fino 49 trees independently of root-to-shoot ABA signalling. Funct. Plant Biol. 39 (5), 366–378.

Pérez-Pérez, J.G., Robles, J.M., García-Sánchez, F., Botía, P., 2016. Comparison of deficit and saline irrigation strategies to confront water restriction in lemon trees grown in semi-arid regions. Agric. Water Manag. 164, 46–57.
Petrie, P.R., Wang, Y., Liu, S., Lam, S., Whitty, M.A., Skewes, M.A., 2019. The accuracy and utility of a low cost thermal camera and smartphone-based system to assess grapevine water status. Biosyst. Eng. 179, 126–139.
Pou, A., Diago, M.P., Medrano, H., Baluja, J., Tardaguila, J., 2014. Validation of thermal indices for water status identification in grapevine. Agric. Water Manag. 134, 60–72.
Puértolas, J., Johnson, D., Dodd, I.C., Rothwell, S.A., 2018. Can we water crops with our phones? Smartphone technology application to infrared thermography for use in irrigation management. XXX Int. Hortic. Congr. IHC2018: Int. Symp. . Water Nutr. Relat. Manag. 1253 443–448.
Ramírez-Cuesta, J.M., Ortuño, M.F., Gonzalez-Dugo, V., Zarco-Tejada, P.J., Parra, M., Rubio-Asensio, J.S., Intrigliolo, D.S., 2022a. Assessment of peach trees water status and leaf gas exchange using on-the-ground versus airborne-based thermal imagery. Agric. Water Manag. 267, 107628.
Ramírez-Cuesta, J.M., Consoli, S., Longo, D., Longo-Minnolo, G., Intrigliolo, D.S., Vanella, D., 2022b. Influence of short-term surface temperature dynamics on tree orchards energy balance fluxes. Precis. Agric. 1–19.
Romero-Trigueros, C., Gambín, J.M.B., Nortes Tortosa, P.A., Cabañero, J.J.A., Nicolás, E. N., 2021. Isohydricity of two different citrus species under deficit irrigation and reclaimed water conditions. Plants 10 (10), 2121.
Rud, R., Cohen, Y., Alchanatis, V., Levi, A., Brikman, R., Shenderey, C., Heuer, B., Markovitch, T., Dar, Z., Rosen, C., Mulla, D., Nigon, T., 2014. Crop water stress index derived from multi-year ground and aerial thermal images as an indicator of potato water status. Precis. Agric. 15 (3), 273–289.
Saitta, D., Vanella, D., Ramírez-Cuesta, J.M., Longo-Minnolo, G., Ferlito, F., Consoli, S., 2020. Comparison of orange orchard evapotranspiration by eddy covariance, sap flow, and FAO-56 methods under different irrigation strategies. J. Irrig. Drain. Eng. 146 (7), 05020002.
Saitta, D., Consoli, S., Ferlito, F., Torrisi, B., Allegra, M., Longo-Minnolo, G., Vanella, D., 2021. Adaptation of citrus orchards to deficit irrigation strategies. Agric. Water Manag. 247, 106734.
Santana-Vieira, D.D.S., Freschi, L., Almeida, L.A.D.H., Moraes, D.H.S.D., Neves, D.M., Santos, L.M.D., Zanelato-Bertolde, F., Soares-Filho, W.S., Coelho-Filho, M.A., Gesteira, A.D.S., 2016. Survival strategies of citrus rootstocks subjected to drought. Sci. Rep. 6 (1), 38775.
Sepaskhah, A.R., Kashefipour, S.M., 1994. Relationships between leaf water potential, CWSI, yield and fruit quality of sweet lime under drip irrigation. Agric. Water Manag. 25 (1), 13–21.
Shafian, S., Rajan, N., Schnell, R., Bagavathiannan, M., Valasek, J., Shi, Y., Olsenholler, J., 2018. Unmanned aerial systems-based remote sensing for monitoring sorghum growth and development. PloS One 13 (5), e0196605.
Takács, S., Pék, Z., Bíró, T., Helyes, L., 2018. Heat stress detection in tomato under different irrigation treatments (June). XV Int. Symp. . Process. Tomato 1233, 47–52.
Vanella, D., Ferlito, F., Torrisi, B., Giuffrida, A., Pappalardo, S., Saitta, D., Longo-Minnolo, G., Consoli, S., 2021. Long-term monitoring of deficit irrigation regimes on citrus orchards in Sicily. J. Agric. Eng. 52 (4).
Vanella, D., Ramírez-Cuesta, J.M., Longo-Minnolo, G., Longo, D., D'Emilio, A., Consoli, S., 2022. Identifying soil-plant interactions in a mixed-age orange orchard using electrical resistivity imaging. Plant Soil 1–17.
Waldo, L.J., Schumann, A.W. , 2009. Alternative methods for determining crop water status for irrigation of citrus groves. In Proceedings of the Florida State Horticultural Society (Vol. 122, pp. 63–71).
Yamada, M., Uematsu, Y., Sasaki, R., 1996. A visual technique for the evaluation of the pedestrian-level wind environment around buildings by using infrared thermography. J. Wind Eng. Ind. Aerodyn. 65 (1), 261–271.